AD-A253 146

REPORT DOCUMENTATIO

roved
0704-0188

(2)

1. AGENCY USE ONLY (Leave blank)	2. REPORT DATE	3. REPORT TYPE AND DATES COVERED
	July 01, 1992	Final Technical 5/15/90-5/14/92

4. TITLE AND SUBTITLE

Control of Lift and Drag in Unsteady Flows

5. FUNDING NUMBERS

F49620-90-C-0038
2307/CS

6. AUTHOR(S)

Ho, Chih-Ming

7. PERFORMING ORGANIZATION NAME(S) AND ADDRESS(ES)

University of Southern California
Department of Aerospace Engineering
University Park, RRB 101
Los Angeles, CA 90089-1191

8. PERFORMING ORGANIZATION REPORT NUMBER

9. SPONSORING/MONITORING AGENCY NAME(S) AND ADDRESS(ES)

Air Force Office of Scientific Research
Bolling AFB, D.C. 20332-6448

N/A

10. SPONSORING/MONITORING AGENCY REPORT NUMBER

F49620-90-C-0038

11. SUPPLEMENTARY NOTES

12a. DISTRIBUTION/AVAILABILITY STATEMENT

Approved for publication and release; distribution unlimited

12b. DISTRIBUTION CODE

13. ABSTRACT (Maximum 200 words)

The response of delta wings with different aspect ratios and a 2-D wing in unsteady free stream was investigated. It was found that the characteristics of the lift forces depend on the existence of leading-edge vortex shedding. For delta wings with attached leading-edge vortex, the time-averaged lift force was found to be independent of reduced frequency since there is no intrinsic vortex convection time scale. With increasing angle of attack or aspect ratio, vortex shedding can occur, and the time required to convect along the chord becomes an intrinsic time scale. The appearance of the instrinsic convection time scale on the delta wing corresponds to increased lift with increasing reduced frequency, just like the 2-D wing. Flow visualizations of vortex breakdown position around the trailing edge does not affect the lift force. For the 2-D wing, the aerodynamic performance in the poststall region shows a maximum at an optimum frequency. Very high lift coefficients exceeding 10 can be observed at this reduced frequency.

14. SUBJECT TERMS	15. NUMBER OF PAGES
Separated flow/lift enhancement	75
	16. PRICE CODE

17. SECURITY CLASSIFICATION OF REPORT	18. SECURITY CLASSIFICATION OF THIS PAGE	19. SECURITY CLASSIFICATION OF ABSTRACT	20. LIMITATION OF ABSTRACT
unclassified	unclassified	unclassified	

Contract No. F49620-90-C-0038

CONTROL OF LIFT AND DRAG IN UNSTEADY FLOWS

Principal Investigator:
Ho, Chih-Ming

Department of Aerospace Engineering
University of Southern California
University Park
Los Angeles, California 90089-1191

June 20, 1992

Final Technical Report
Period: May 15, 1990 to May 14, 1993

Air Force Office of Scientific Research
Bolling Air Force Base
Washington, D.C. 20332-6448

1. PURPOSE

The purpose of this project is to study the unsteady response of stationary 2-D and 3-D airfoils in a periodically varying free stream. First, we wish to understand the mechanism for vorticity generation and transport and examine how it dominates the unsteady behavior of two- and three-dimensional separating lifting surfaces. We examined the effect of different parameters, such as aspect ratio, reduced frequency and acceleration time. We will then develop and apply appropriate control techniques to enhance the post-stall operation of a 2-D airfoil. Finally, we will also implement future experiments to examine the unsteady aerodynamic loading produced by a pitching delta wing in unsteady free streams.

2. ACCOMPLISHMENTS

2.1 Aerodynamics of Attached Unsteady Flow Around 2-D Airfoil

When the flow on the 2-D airfoil is attached, the vorticity convection is balanced by a part of the vorticity diffusion. Hence, the convected vorticity does not play a role in the dynamics. The lift is determined by the remainder of the vorticity diffused from the surface.

2.2 Aerodynamics of Vortical Flows in Unsteady Free Stream

The response of delta wings with different aspect ratios and a 2-D wing in unsteady free stream was investigated. When an airfoil is placed in an unsteady free stream, two important time scales exist: an intrinsic vortex convection time scale and an external perturbation time scale. The convection time scale is a measure of the time needed for a vortex to pass the airfoil. This physical interpretation is meaningful only when vortex shedding from the leading edge takes place. The reduced frequency is the ratio of the convective time scale and the external perturbation time scale. For the smallest aspect ratio delta wing investigated (AR=1), the time-averaged lift force was found to be independent of reduced frequency for a large range of angles of attack. The independence of the lift force from the reduced frequency implies that there is no intrinsic time scale as long as the leading-edge vortices are attached.

Unlike the AR=1 delta wing, the time-averaged lift force is a strong function of the reduced frequency for the 2-D wing in the post-stall region. This is because the intrinsic vortex convection time scale plays an important role. However, when the flow is attached for small

angle of attack, there is no convected vortex, and the lift is not a function of the reduced frequency any longer. The response of delta wings at aspect ratios higher than one has transitional behavior between a 2-D wing and the AR=1 delta wing. When the aspect ratio or angle of attack is increased, the convection of vorticity along the cores of the leading edge vortices in the streamwise direction decreases. As the accumulated vorticity increases, the leading edge vortices start shedding and the intrinsic convection time scale appears on the delta wing. The appearance of the intrinsic convection time scale on the delta wing corresponds to increased lift with increasing reduced frequency, just like the 2-D wing. Therefore, we may conclude that the characteristics of the lift forces depend on the existence of leading-edge vortex shedding.

The aerodynamic performance (both time-averaged and phase averaged) of the 2-D wing in the poststall region shows a maximum at an optimum frequency. The optimum reduced frequency does not depend on the amplitude of oscillation and is approximately independent of angle of attack. Very high lift coefficients exceeding 10 can be observed at this reduced frequency. This high performance is due to a large coherent vortex which sheds from the leading edge and remains on the wing until the time when the free stream velocity is minimum. The optimum reduced frequency does not seem to be related to wake instability, although the natural vortex shedding frequency and the optimum frequency are of the same order of magnitude. Finally, the observed high aerodynamic loads does not critically depend on the curvature of the leading-edge.

Although no unsteady force measurements were taken for drag, the time-averaged value was estimated from wake velocity measurements. The average drag force also shows a maximum at the optimum reduced frequency. However, the average drag force increases less rapidly with increasing reduced frequency than the average lift force does. This is most probably due to the reversed flow (hence negative skin friction) over the wing during the time interval when the vortex is located above the wing.

2.3 Vortex Breakdown in Unsteady Free Stream

Air bubbles were entrained into the vortex cores on delta wings, which provided a way to visualize leading edge vortices. The motion was videotaped and studied in detail. The analysis shows that the vortex cores in a given cross section remain at a fixed position during the cycle. The burst position may vary depending upon its steady state location. Flow visualization shows that the burst location is not affected, if it is away from the trailing-edge and closer to the apex in

the steady free stream. Otherwise, the breakdown position may move onto the wing during the acceleration phase of the free stream, depending on the frequency and amplitude. On the other hand, lift measurements showed that the time-averaged lift force does not change with angle of attack in this range. Therefore, this suggests that the change in vortex breakdown position around the trailing edge does not effect the lift force.

From flow visualization, a sudden jump in the breakdown position was observed during the acceleration of the free stream. Detailed phase-averaged velocity measurements along the core showed that the axial velocity undergoes a transition from a jet-like to a wake-like profile during the acceleration. This wake-like profile is replaced by a jet-like one as the breakdown is washed downstream. Variation of swirl angle and circulation are shown to be unaffected by the movement of the breakdown. It is argued that the time-dependent nature of burst position is due to the variation of pressure on the wing surface. The acceleration of the free stream produces more adverse pressure gradients in a region near the trailing-edge due to the Kutta condition, causing earlier breakdown. This explanation is consistent with the experimental observations that the sensitivity of the breakdown decreases if it is closer to the apex (roughly less than half-chord length from the apex). The importance of the trailing-edge has been determined from breakdown in steady free stream; the burst position is extremely sensitive to the angle of attack and leading-edge shape when it is around the trailing-edge. Together, these evidences support the explanation that vortex breakdown over unsteady delta wings is a pressure driven phenomena.

3. AWARDS

1990 Prize winner of the Eighth Annual Picture Gallery of Fluid Motions, American Physical Society, 43rd Annual Meeting, Division of Fluid Dynamics, November 18-20, Cornell University, Ithaca, New York.

4. PUBLICATIONS

Lee, M.and Ho, C.M. 1990 Lift force of delta wings, *Applied Mechanics Reviews*, vol. 43, pp. 209-221.

Gursul, I., Lin, H. and Ho, C.M. 1991 An airfoil with $C_L > 10$, *Physics of Fluids A*, Gallery of Fluid Motion, vol. 3, no. 9, p. 2030.

Gursul, I. and Ho, C.M. 1992 High aerodynamic loads on an airfoil submerged in an unsteady stream, *AIAA Journal*, vol. 30, no. 4, pp. 1117-1119.

Gursul, I., Lin, H. and Ho, C.M. Vortex dynamics of separated flow over an airfoil in unsteady free stream, *in preparation for publication*

Gursul, I., Lin, H. and Ho, C.M. Vortex dynamics of delta wings in unsteady free stream, *in preparation for publication.*

Gursul, I., Lin, H. and Ho, C.M. Vortex breakdown over delta wings in unsteady free stream, *in preparation for publication.*

5. CONFERENCES AND WORKSHOPS

Gursul, I., Lin, H. and Ho, C.M. 1990 An airfoil with C_L>10, *Bulletin of the American Physical Society*, Vol. 35, No. 10, p. 2318.

Ho, C.M., Gursul, I., Shih, C. and Lin, H. 1990 Vorticity balance on 2-D and 3-D unsteady airfoils, Workshop on Physics of Forced Unsteady Separation, NASA Ames Research Center

Gursul, I., Lin, H. and Ho, C.M. 1991 Vorticity dynamics of 2-D and 3-D wings in unsteady free stream, AIAA Paper 91-0010, 29th Aerospace Science Meeting, January 7-10, Reno, Nevada.

Bao, Y., Gursul, I. and Lee, C.J. 1991 Computational study of an unsteady, separated 2-D flow and vortex lift at low Mach number, 4th International Symposium on Computational Fluid Dynamics, September 9-12, Davis, California.

Gursul, I., Lin, H. and Ho, C.M. 1991 Vortex dynamics of delta wings in unsteady free stream, *Bulletin of the American Physical Society*, vol. 36, no. 10, p. 2702.

Gursul, I. 1992 Vortex break down in unsteady flows, AFOSR Workshop on Supermaneuverability: Physics of Unsteady Flows Past Lifting Surfaces at High Angle of Attack, Lehigh University, April 9-10.

Ho. C.M., Lin, H. and Gursul, I. 1992 Delta Wings in Unsteady Flows, the Fifth Asian Congress of Fluid Mechanics, Korea, August 10-14.

VORTEX BREAKDOWN OVER DELTA WINGS IN UNSTEADY FREE STREAM

Ismet Gursul, Hank Lin and Chih-Ming Ho
Department of Aerospace Engineering
University of Southern California
Los Angeles, California 90089-1191

ABSTRACT

Time-dependent nature of vortex breakdown over delta wings in an unsteady periodic free stream was investigated. Flow visualization shows that the burst location is not affected, if it is away from the trailing-edge and closer to the apex in steady free stream. Otherwise, the breakdown position may move onto the wing during the *acceleration* of the free stream, depending on the frequency and amplitude. Phase-averaged LDA velocity measurements show that axial velocity undergoes a transition from jet-like to wake-like profile during the breakdown process. This wake-like profile is replaced by a jet-like one as the breakdown is washed downstream. Variation of swirl angle and circulation are shown to be not influenced by breakdown. It is argued that the time-dependent nature of burst position is due to the variation of pressure on the wing surface.

INTRODUCTION

While the interest in unsteady aerodynamics of delta wings is increasing, the vortex breakdown remains a challenging aspect of the vortical flow fields. The practical importance of vortex breakdown has increased because of use of delta wings in modern aircraft. Since highly maneuverable aircraft is designed to operate at high angle of attack, the breakdown may move on the wing and affect the stability of aircraft.

While the breakdown is in the wake for small angle of attack in steady free stream, it occurs on the wing and moves toward the apex with increasing angle of attack. However, this is not necessarily the case for unsteady flows. For a pitching delta wing, there is a phase shift between the motion of the wing and breakdown location. The phase angle mainly depends on the reduced frequency[1] and can be as large as 180° (which means that the breakdown moves toward the apex as the angle of attack *decreases*[2]).

The physical mechanism responsible for breakdown is not well understood even in steady free

stream conditions. The reviews by Leibovich[3] and Hall[4] suggest that there are several theories to explain the phenomena. The early studies of breakdown used flow visualization extensively and most of these studies were conducted in tubes. The vortex over a delta wing is different than the tube vortex because of continuous feeding of vorticity from the leading-edge and growth in axial direction. Velocity measurements of breakdown with nonintrusive techniques such as Laser Doppler Anemometer (LDA) made quantitative flow information avaible. It was observed that the axial velocity profiles are jet-like before the breakdown and becomes wake-like after the breakdown[5]. The measurements suggest that the breakdown occurs when the swirl angle ($\phi=\tan^{-1}(v/u)$, where v and u are the swirl and axial components of velocity respectively) reaches a critical value[6,7], larger than 40°. However, even at small swirl angles, it is possible to induce vortex breakdown by imposing an adverse pressure gradient. For example, placing an object on the axis will cause an earlier breakdown. It was suggested by Hall[4] that vortex breakdown occurs depending on "a balance between the magnitude of the swirl, the external pressure gradient, and the degree of divergence of the flow". He also showed that small external pressure gradients can be amplified along the core of the vortices, leading to a stagnation point. This amplification of adverse pressure gradient along the axis was demonstrated experimentally as well[8].

In this study, vortex breakdown characteristics over delta wings in an unsteady stream was investigated. Experiments were conducted on two delta wings (aspect ratio A=1 and 2). Characteristics of breakdown and its time-dependent behaviour were documented by flow visualization and LDA measurements.

EXPERIMENTAL FACILITY

Experiments were conducted in a vertical unsteady water channel with a cross-sectional area of 45.7 by 45.7 cms. The free stream control was achieved by rotating a gate (which operates like a valve) downstream of the test section. The rotation of the gate is done with a computer controlled stepping motor. The principle and process of controlling the free stream is explained in detail elsewhere[9]. This channel-gate combination provides a large range of amplitude and frequency of the time-varying free stream with different types of waveforms. Another important application is the transient experiments. For the oscillating free stream, the velocity can be represented in the form of:

$$U/U_\infty = 1+R\cos\omega t = 1+R\cos 2\pi t/T \qquad (1)$$

where U_∞ is the average velocity, R is the dimensionless amplitude ($R<1$) and $\omega=2\pi/T$ is the radial frequency. The free stream turbulence level was about 0.5%.

The velocity field was measured with a two-component Laser Doppler Anemometer (LDA)

(DANTEC, 55X optical system) operated in forward-scattering mode and equipped with a 100 mW Argon-Ion laser (Ion Laser Technology) and two LDA counters (DANTEC 55L96). The optical system was equipped with a beam expander, a 310 mm focusing lens and bragg cell for frequency shifting. The nominal measuring volume was estimated to be about 0.1 mm in diameter and 1 mm in length. Velocity measurements across the vortex core were made with a spacing as small as Δy=1 mm. These measurements were repeated at different streamwise locations spaced as Δx=1 cm ($\Delta x/c \simeq 0.036$), covering a domain roughly half-chord length from the trailing-edge. Velocity signals were digitized by an analog-to-digital converter (RC Electronics, model ISC-67) and processed by an UNIPAQ 386 personal computer. Ensemble-averaging technique was applied to the signals to extract deterministic parts. An average of 50 cycles with 100 points per cycle were averaged.

Different sharp-edged delta wings were used for flow visualization and LDA measurements. For flow visualization, the chord lengths were c=20 cm for A=1 and c=17 cm for A=2. The blockage ratio was 0.044 at the maximum angle of attack α=40°. For LDA measurements, an aspect ratio A=1 wing with c=28 cm was used. At a maximum angle of attack α=28°, the blockage ratio was 0.04. The Reynolds number was in the range of 30,000 to 60,000 for all airfoils. The leading-edge was beveled with a 30° angle.

Flow visualization was carried out by illuminating air bubbles which were entrained into the vortex cores on delta wings, providing a way to visualize leading-edge vortices. A tungsten light source made of two 500 W lamps with a slit as well as a laser sheet scanned by a mirror was used to iilluminate the flow field. A 35 mm camera (NIKON, model F-2) was used in taking still pictures. This camera could be triggered by a pulse at any particular time which is phase-referenced to the pulse train used for the rotating gate. The time-dependent flow field was also videotaped using a CCD camera (ELMO, model SE301) and a VCR (Panasonic S-VHS). In order to provide a reference, a LED indicator was used.

RESULTS

While the vortex breakdown might be in the far wake in steady free stream, it can be observed on the wing with increasing unsteady effects. As an example, effect of the amplitude on flow visualization for A=1 delta wing at α=25° is shown in figure 1. The reduced frequency, $k=\omega c/2U_\infty$=1.395, (where c is the chord length) is the same for both columns. It is seen that, when the free stream velocity is maximum (t/T=0), the breakdown is on the wing. In fact, the breakdown starts during the acceleration and is washed downstream during the deceleration (see t/T=0.25). The size of the core after the breakdown increases with increasing amplitude R. In general, increasing unsteady effects (frequency or amplitude) have been found to cause breakdown earlier and more intense, even if there is no breakdown on the wing in steady free stream case.

The effect of geometry (angle of attack and sweep angle) has been studied for constant reduced frequency and amplitude. Results of flow visualization have been summarized in figure 2, which indicates two important observations. First of all, the vortex breakdown position is not influenced by the unsteadiness when it is closer to the apex (less than a half-chord distance). Secondly, during the acceleration ($t/T \approx 0.8$), the breakdown position jumps to an upstream location regardless of angle of attack and aspect ratio (if it is not closer to the apex). During the deceleration, breakdown is washed downstream with a convection velocity $U_C \approx 0.2\ U_\infty$. It should be noted that the exact moment of the jump is difficult to determine because of the nature of flow visualization. Furthermore, for small angles of attack, the vortex core after the breakdown is small compared to that of the steady free stream case. This makes the determination of breakdown position by flow visualization difficult. These observations of vortex breakdown in periodic free stream are consistent with Lambourne and Bryer's[10] observations in accelerated and decelarated free stream. By suddenly changing the tunnel speed, they observed that the burst position moved *upstream* during *acceleration* and slowly returned to its steady state position. The opposite behaviour was observed in decelerating free stream. These results were confirmed in this unsteady water facility which allowed us to carry out well-controlled transient experiments. It is also interesting to note that, in the case of vortex tube experiments, the effects of transient free stream were opposite to those for a delta wing vortex[10]. This behaviour for vortex tube experiments was attributed to the shedding of starting or stopping vortices from swirl vanes[11].

In order to understand the nature of unsteady breakdown process, measurements of velocity components parallel and normal to the wing surface were taken in the plane of the vortex core centers (figure 3). Since the measurements were taken along a traverse line parallel to the trailing edge (which is not perpendicular to the vortex axis), they approximately correspond to the axial and swirl velocities across the vortex core. From phase-averaged measurements taken at different streamwise stations, the velocity field along the vortex core was constructed and presented in figure 4 for $\alpha=28^\circ$. The axial velocity distribution (normalized by U_∞) shows an abrupt transition from a jet-like to a wake-like profile across the breakdown region. During the deceleration ($t/T \geq 0$), the breakdown moves downstream. After the breakdown leaves the wing, a jet-like velocity profile is observed everywhere. During the acceleration, a change starts to take place around $t/T=0.75$. It is obvious from the velocity profile that as the free stream increases, there is not a corresponding increase in the core. The transition occurs everywhere simultaneously and wake-like velocity profile developes eventually. As will be shown later, the swirl angle for this case is around 50°, which is in the range of the reported values $\phi = 40^\circ - 55^\circ$ for breakdown[4,7].

It is possible to have vortex breakdown even at lower angle of attacks (lower swirl angles), if the reduced frequency is high enough. The results of measurements at $\alpha=15^\circ$ is shown in figure 5. The

axial velocity distribution (normalized by U_∞) is qualitatively similar to that of figure 4, although the breakdown seems less intense. In this case, the maximum swirl angle is approximately ϕ=30° and remains roughly constant throughout the cycle. While there is no breakdown in *steady* free stream in both cases (figure 4 and 5), the burst is induced by the unsteadiness. However, the breakdown seems very mild compared to the case of stationary or pitching delta wing[2], based on the velocity measurements. A measure of the abrupt deceleration can be obtained by centerline velocity gradient in the breakdown region. This quantity $\partial u/\partial x$ (x, r=0)$\simeq$10 U_∞/c (negative sign omitted) for stationary or pitching delta wing, whereas $\partial u/\partial x$ (x, r=0)$\simeq$2 U_∞/c for the case in figure 5.

Because of the possibility that the vortex core may be slightly moving out of measurement plane during the cycle (there are no large movements based on flow visualization), the figures 4 and 5 should be considered carefully. In order to get a three-dimensional picture, detailed measurements in a cross plane (x/c=-0.25) were taken. The measurement region is shown for α=15° in figure 6. The normalized axial velocity is shown at different phases of the cycle in figure 7. Although the location of the extremum of the axial velocity changes slightly during the cycle, it is seen that the variations in cross-plane is consistent with the variations along the core. Therefore, the cuts along the core are representative of three-dimensional development. Figure 8 shows the variation of normalized swirl velocity along the vortex core for the case in figure 5 (α=15°). The swirl velocity shows less variations during the cycle and little with breakdown. Although there is a big change in the slope in the y-direction (which is approximately the vorticity) before and after the breakdown, it is not visible in the scale of the figure.

It is seen that the observed variations in the axial velocity field start around t/T=0.75 when the acceleration is maximum. This can be seen clearly from the time history of velocity shown in figure 9 (corresponding to figure 5). The breakdown starts around t/T=0.75 in all stations, however the magnitude of the variations depends on the location. At the very upstream location (top of the figure 9), there is little effect due to the breakdown. The duration of wake-like profile at a given streamwise location depends on the time when the breakdown is washed away from that station. While the velocity outside the wing varies like free stream, the variation in the core seems limited by breakdown.

Since drastic changes take place in the core during the breakdown, its effect on global quantities such as circulation is a main interest. For this reason, circulation measurements were carried out around a closed path (shown at top of figure 10) at each streamwise location. The dimensionless circulation $\Gamma/U_\infty c$ is shown as a function of streamwise distance and time at the bottom of figure 10. The circulation seems to be varying in harmony with the free stream at any x-station. It is also approximately linear function of streamwise distance, except in a region very close to the trailing-edge. (The circulation in a conical flow field would also give a linear variation). Also shown in x-t plane is

the movement of the breakdown. (At any point downstream of the solid line, a wake-like velocity exists. In the shaded time interval, the transition from jet-like to wake-like profile takes place). The conclusion from this figure is that the variation of circulation is not influenced by the breakdown.

DISCUSSION OF RESULTS

All the results presented here show that, during the *acceleration*, the vortex breakdown starts at an upstream location. This seems to be in contrary to the expectation, because an acceleration (whicn is identical to a favorable pressure gradient) leads to an earlier breakdown.

It is of interest to consider this behaviour from the view of Hall's theory. Hall suggested that vortex breakdown occurs as a result of adverse pressure gradient along the centerline which leads to a stagnation point. In a sense, it is analogous to boundary layer separation. He shows that there are two possible ways to produce an adverse gradient: an external adverse pressure gradient and a divergent flow. With the assumption of quasi-cylindrical flow (which is a reasonable approximation before the breakdown),

$$\frac{\partial p}{\partial x}(x, r=0) = \frac{\partial p}{\partial x}(x, r=R) - \int_0^R \frac{\partial}{\partial x}\left(\frac{\rho v^2}{r}\right) dr \qquad (2)$$

In this equation, x is the streamwise distance, r is the radius being measured from the center of the vortex and R is the edge of the vortex where the external boundary conditions exist. (It should be noted that the quasi-cylindrical assumption requires that the equation (2) is still valid in unsteady flows[12]). The first term is the external pressure gradient and second term is the contribution due to the swirl component. For delta wing vortices, the pressure on the suction surface of the wing can be considered as the external field (although it is not axisymmetric). This external pressure gradient is generated by the wing and is an adverse one due to Kutta condition at the trailing edge. The pressure measurements on delta wings is consistent with this description[10].

Hall shows that, if the stream surfaces diverge, the pressure gradient along the axis will be more adverse than the external pressure gradient according to the equation (2). For delta wing flows, the continuous feeding of vorticity leads to the growth of the core, which produces divergent stream surfaces. The contribution due to the swirl component is related to the swirl angle, which confirms the observations that an increase in swirl angle causes an earlier breakdown. It is of interest to study the variation of swirl angle in unsteady free stream conditions. In figure 11, the vorticity and swirl angle distribution at time t/T=0.125 of figure 4 are shown. The vorticity was estimated from the swirl velocity measurements across the core. It is seen that the high vorticity is confined to the "subcore" region before the breakdown and the core expands after the breakdown. However, the maximum swirl

angles (before and after the breakdown) does not change much. If the maximum swirl angle is plotted as a function of the streamwise distance and time (figure 12), this quantity seems pretty much constant. Again the solid line in x-t plane denotes the movement of the breakdown. This figure suggests that the maximum swirl angle is not correlated with the movement of the vortex breakdown. This brings the possibility that the dynamic character of the breakdown might be due to the variation of pressure on the wing surface. The acceleration in the free stream does not necessarily produce a favorable pressure gradient on the wing. For example, the calculated pressure variation on a thin 2-D airfoil in unsteady free stream[13] shows that the largest changes (with respect to the steady free stream) occur in a region near the trailing-edge (25% chord length from the trailing-edge). Furthermore, the maximum adverse pressure gradient in this region occurs during the acceleration ($t/T \simeq 0.625$) for the parameters in figure 2. These calculations for infinite aspect ratio should provide a good approximation since the essential features of breakdown are the same for a larger aspect ratio wing (A=2) as well. Because the potential flow contribution increases rapidly with increasing aspect ratio according to the Pohlhamus theory[14]. For example, at $\alpha=20^{\circ}$, the potential lift is twice as the vortex lift for A=2 delta wing.

CONCLUSIONS

The vortex breakdown characteristics over delta wings in an unsteady stream was investigated. Flow visualization revealed that the breakdown is observed on the wing with increasing unsteady effects, even if no breakdown is observed on the wing in steady free stream. The effects of the unsteadiness is not felt if the breakdown position (in the steady case) is away from the trailing-edge and closer to the apex. Based on flow visualization, a sudden jump in the breakdown position was observed during the acceleration of the free stream. Detailed phase-averaged velocity measurements along the core showed that the axial velocity undergoes a transition from jet-like to wake-like profile during the acceleration. The centerline velocity gradients along the burst region are several times smaller than those of breakdown is steady free stream. After the wake-like profile developes everywhere (downstream of breakdown location), it is washed downstream. The maximum swirl angle during this process does not change much with the streamwise distance and time. It is argued that dynamic character of burst position is due to variations of pressure on the wing surface. The acceleration of free stream produces more adverse pressure gradients in a region near the trailing-edge (due to the Kutta condition), causing earlier breakdown. This explanation is consistent with the experimental observation that the sensitivity of the breakdown decreases if it is closer to the apex (roughly less than half-chord length from the apex). The importance of trailing-edge was also observed for breakdown in steady free stream; the burst position is extremely sensitive to angle of attack[10] and leading-edge shape[15] when it is around the trailing-edge. All these evidence are in support of the

explanation that the breakdown over unsteady delta wings is a pressure driven phenomena.

ACKNOWLEDGEMENT

This work is supported by AFOSR Contract No. F49620-~~88-C-0061~~ 90-C-0038.

REFERENCES

1. LeMay, S.P., Batill, S.M. and Nelson, R.C. "Vortex dynamics on a pitching delta wing", *Journal of Aircraft*, Vol. 27, No.2, February 1990, pp. 131-138.

2. Atta, R. and Rockwell, D. "Leading-edge vortices due to low Reynolds number flow past a pitching delta wing", *AIAA Journal*, Vol. 28, No. 6, June 1990, pp. 995-1004.

3. Leibovich, S. "Vortex stability and breakdown: survey and extension", *AIAA Journal*, vol. 22, no. 9, 1984, pp. 1192-1206.

4. Hall, M.G. "Vortex breakdown", *Annual Review of Fluid Mechanics*, Vol. 4, 1972, pp. 195-218.

5. Payne, F.M., Ng, T.T. and Nelson, R.C. "Visualization and wake surveys of vortical flow over a delta wing", *AIAA Journal*, Vol. 26, No.2, 1988, pp. 137-143.

6. Wedemeyer, E. "Vortex breakdown", High angle-of-attack aerodynamics, AGARD No. 121, 1982.

7. Lee, M. and Ho. C.M., "Lift force of delta wings", *Applied Mechanics Reviews*, vol. 43, no.9, September 1990, pp. 209-221.

8. Delery, J., Horowitz, E., Leuchter, O. and Solignac, J.L. "Fundamental studies on vortex flows", La Recherche Aerospatiale, No. 2, 1984, pp. 81-104.

9. Gursul, I., Lin, H. and Ho, C.M. "Vorticity dynamics of 2-D and 3-D wings in unsteady free stream", AIAA Paper 91-0010, January 1991.

10. Lambourne, N.C. and Bryer, D.W. "The bursting of leading edge vortices-Some observations and discussion of the phenomenon", Aeronautical Research Council, R. & M. No. 3282, 1962.

11. Faler, J.H. and Leibovich, S. "Disrupted states of vortex flow and vortex breakdown", *The Physics of Fluids*, vol. 20, no. 9, 1977, pp. 1385-1400.

12. Hall, M.G. "The structure of concentrated vortex cores", *Progress. Aero. Sci.*, vol. 7, 1966, pp. 53-110.

13. James, E.C. "A note on flapping flight with surging", Swimming and Flying in Nature, Vol. 2, edited by Wu et al., 1974, Plenum Press, pp. 919-937.

14. Polhamus, E.C. "Prediction of vortex-lift characteristics by leading-edge suction analogy", *Journal of Aircraft*, Vol. 8, No. 4, 1971, pp. 193-199.

15. Panton, R.L. "Effects of a contoured apex on vortex breakdown", *Journal of Aircraft*, vol. 27, no. 3, 1990, pp. 285-288.

LIST OF FIGURES

Figure 1: Flow visualization of vortex breakdown for different amplitudes, A=1, α=25°, k=$\omega c/2U_\infty$=1.395.

Figure 2: Variation of vortex breakdown position for different wings and angles of attack. k=0.93, R=0.42.

Figure 3: Schematics of vortex over delta wing and traverse line across the core.

Figure 4: Axial velocity across the core at different phases of the cycle, α=28°, A=1, k=1.27, R=0.42.

Figure 5: Axial velocity across the core at different phases of the cycle, α=15°, A=1, k=1.27, R=0.42.

Figure 6: Measurement region in a cross plane (x/c=-0.25) for α=15°.

Figure 7: Axial velocity in cross plane at different phases of the cycle, α=15°, A=1, k=1.27, R=0.42 (as in figure 5).

Figure 8: Swirl velocity across the core at different phases of the cycle, α=15°, A=1, k=1.27, R=0.42. (as in figure 5).

Figure 9: Time history of axial velocity across the core at different streamwise locations, α=15°, A=1, k=1.27, R=0.42 (as in figure 5).

Figure 10: Path for circulation measurements and variation of dimensionless circulation as a function of streamwise distance and time, α=28°, A=1, k=1.27, R=0.42 (as in figure 4).

Figure 11: Vorticity (top) and swirl angle (bottom) as a function of distance from the vortex center at time t/T=0.125, α=28°, A=1, k=1.27, R=0.42 (as in figure 4).

Figure 12: Variation of maximum swirl angle as a function of streamwise distance and time, α=28°, A=1, k=1.27, R=0.42 (as in figure 4).

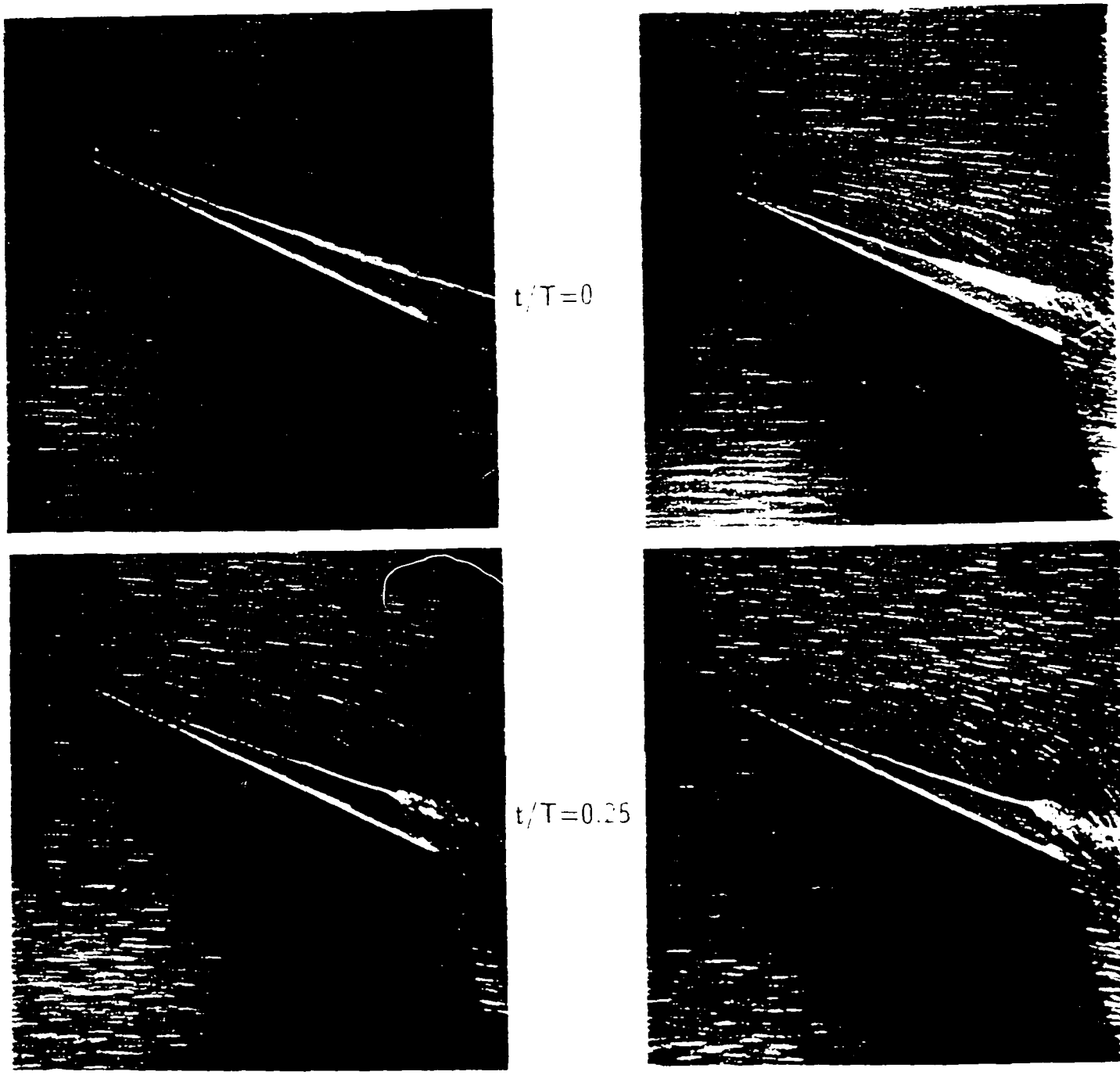

of vortex breakdown

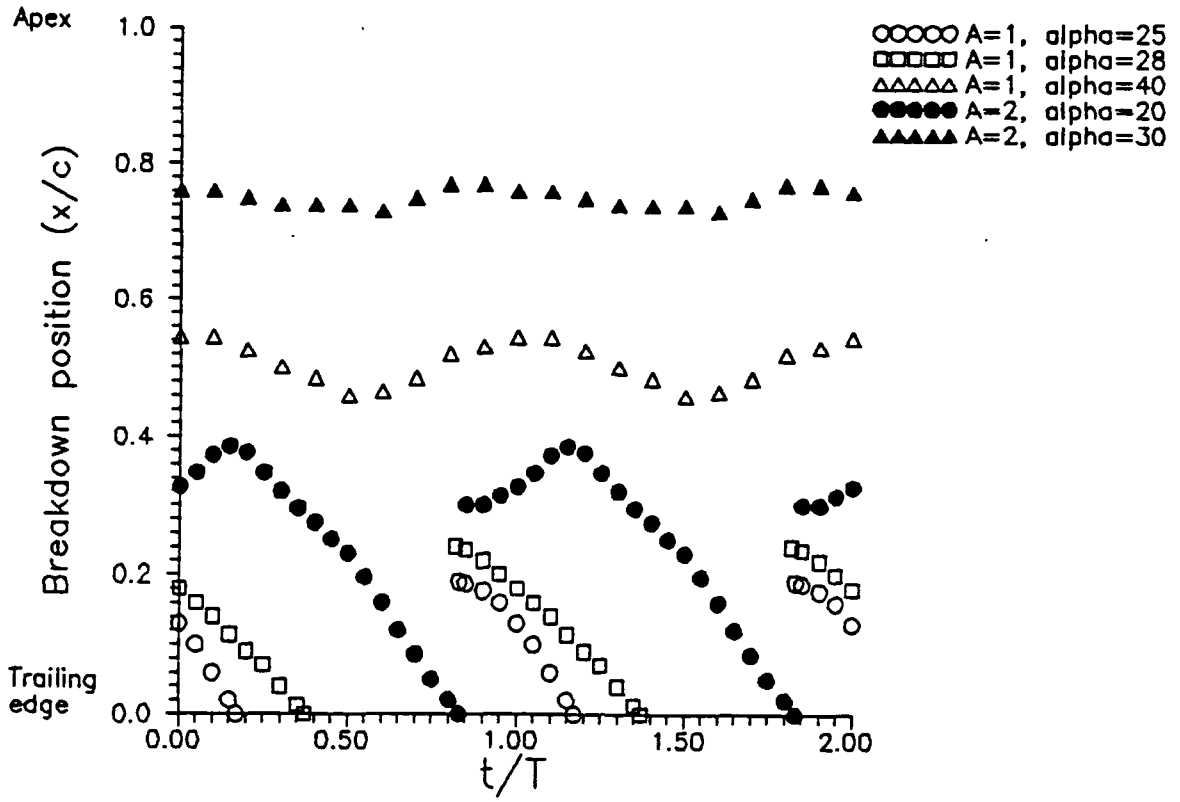

Figure 2: Variation of vortex breakdown position for different wings and angles of attack, k=0.93, R=0.42.

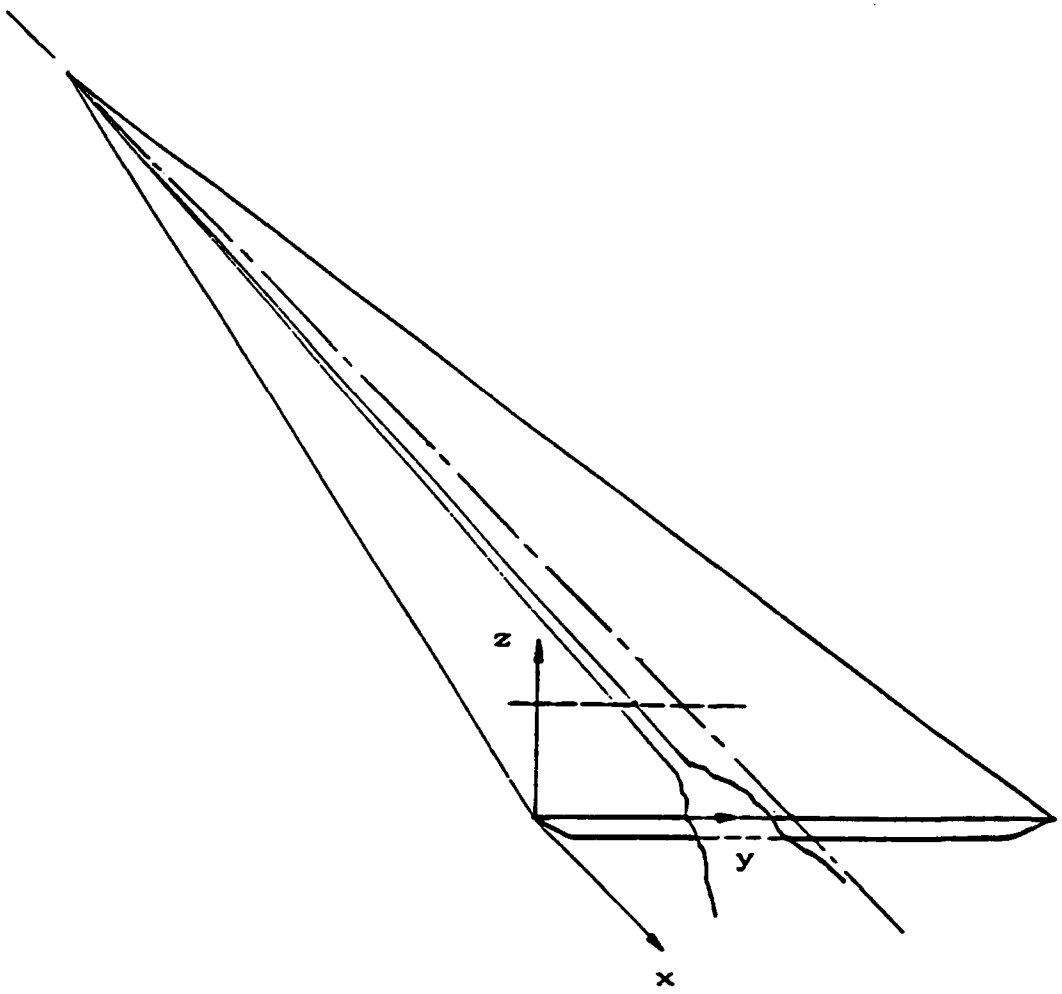

Figure 3: Schematics of vortex over delta wing and traverse line across the core.

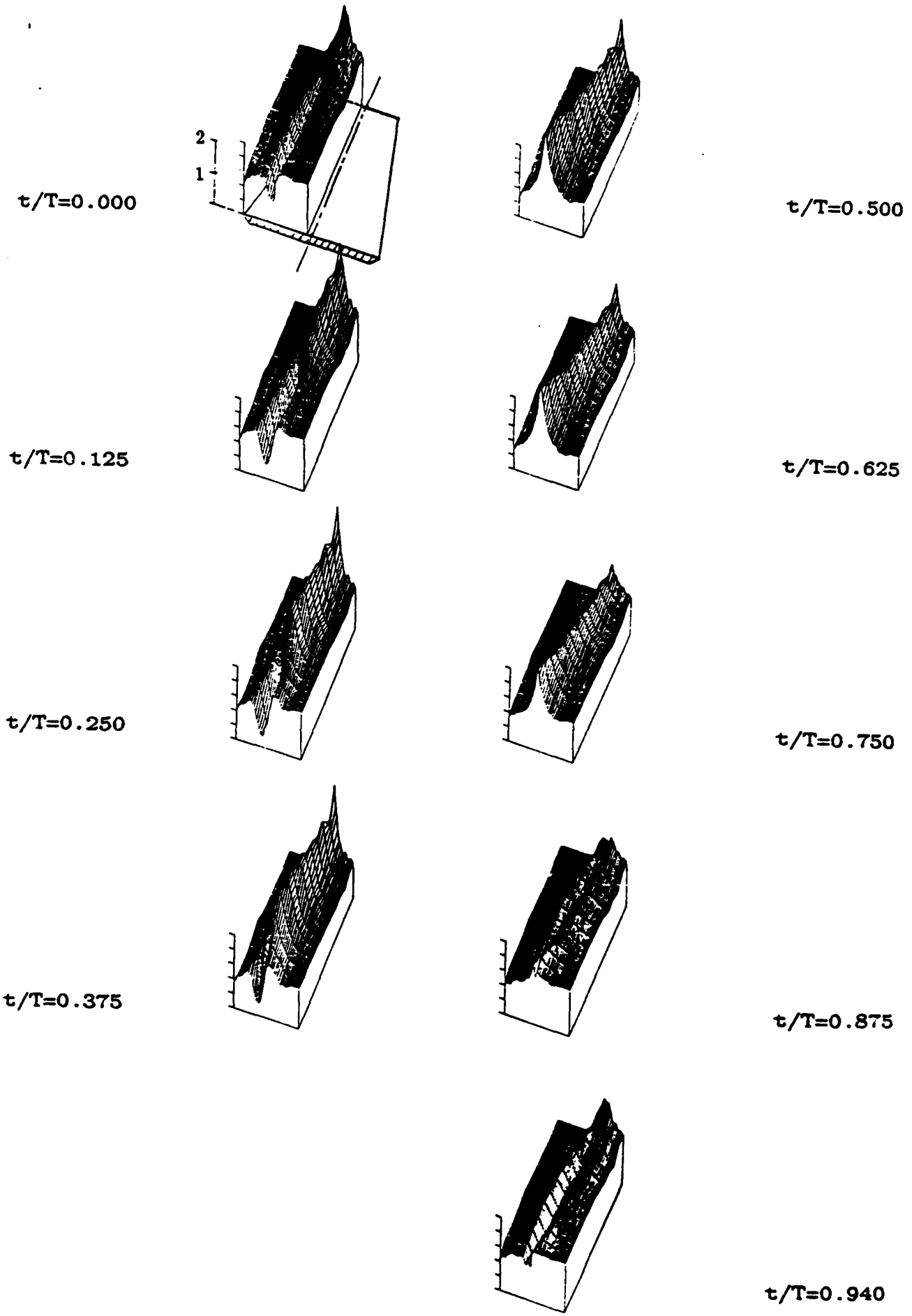

Figure 4: Axial velocity across the core at different phases of the cycle, α=28°, A=1, k=1.27, R=0.42.

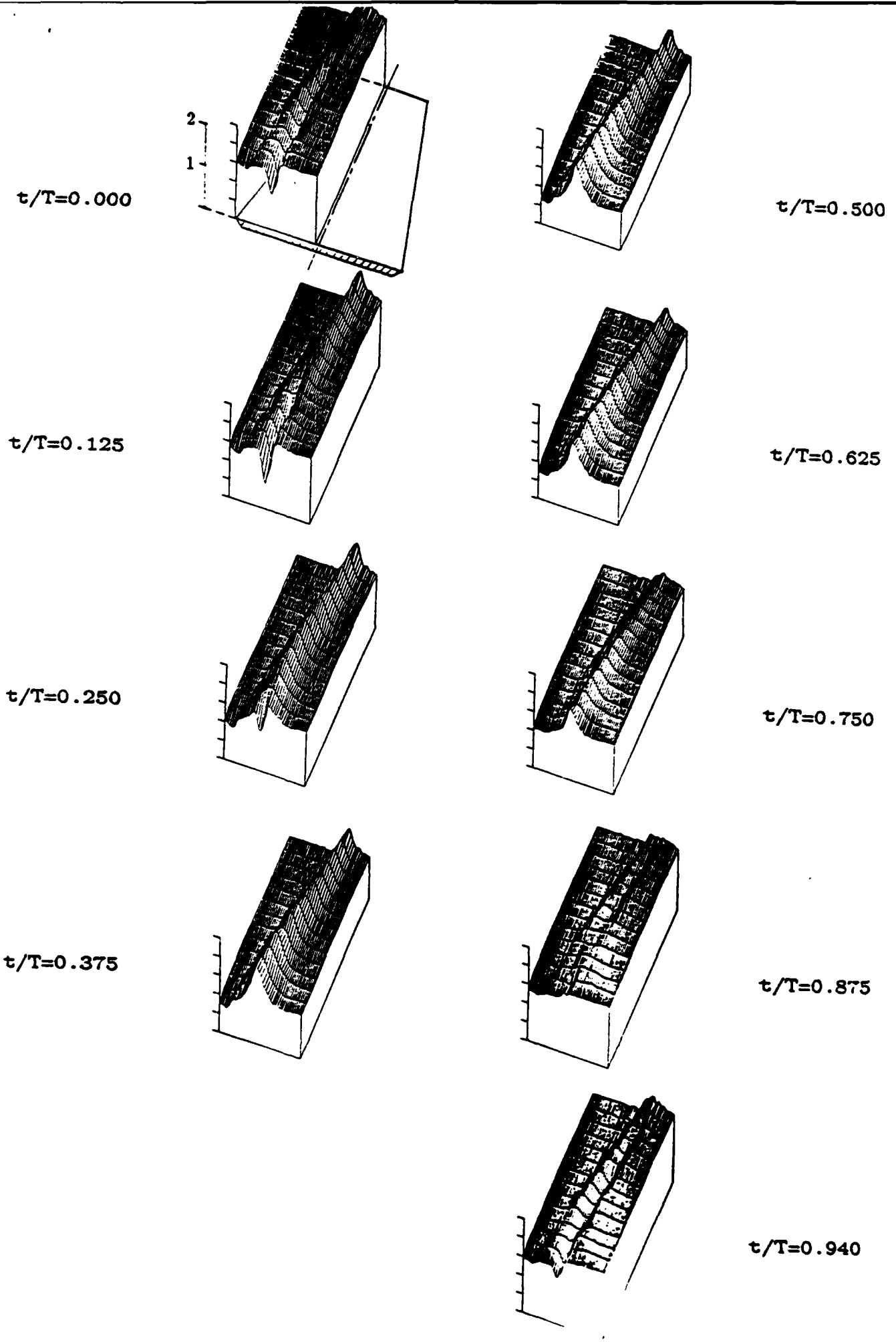

Figure 5: Axial velocity across the core at different phases of the cycle, α=15°, A=1, k=1.27, R=0.42.

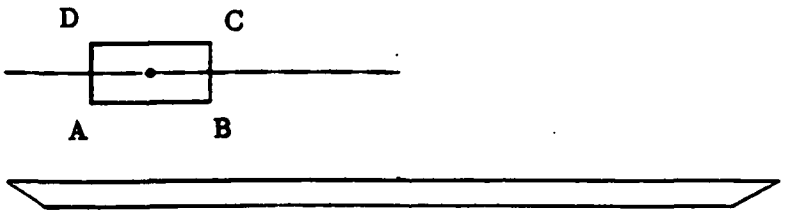

Figure 6: Measurement region in a cross plane (x/c=-0.25) for α=15°.

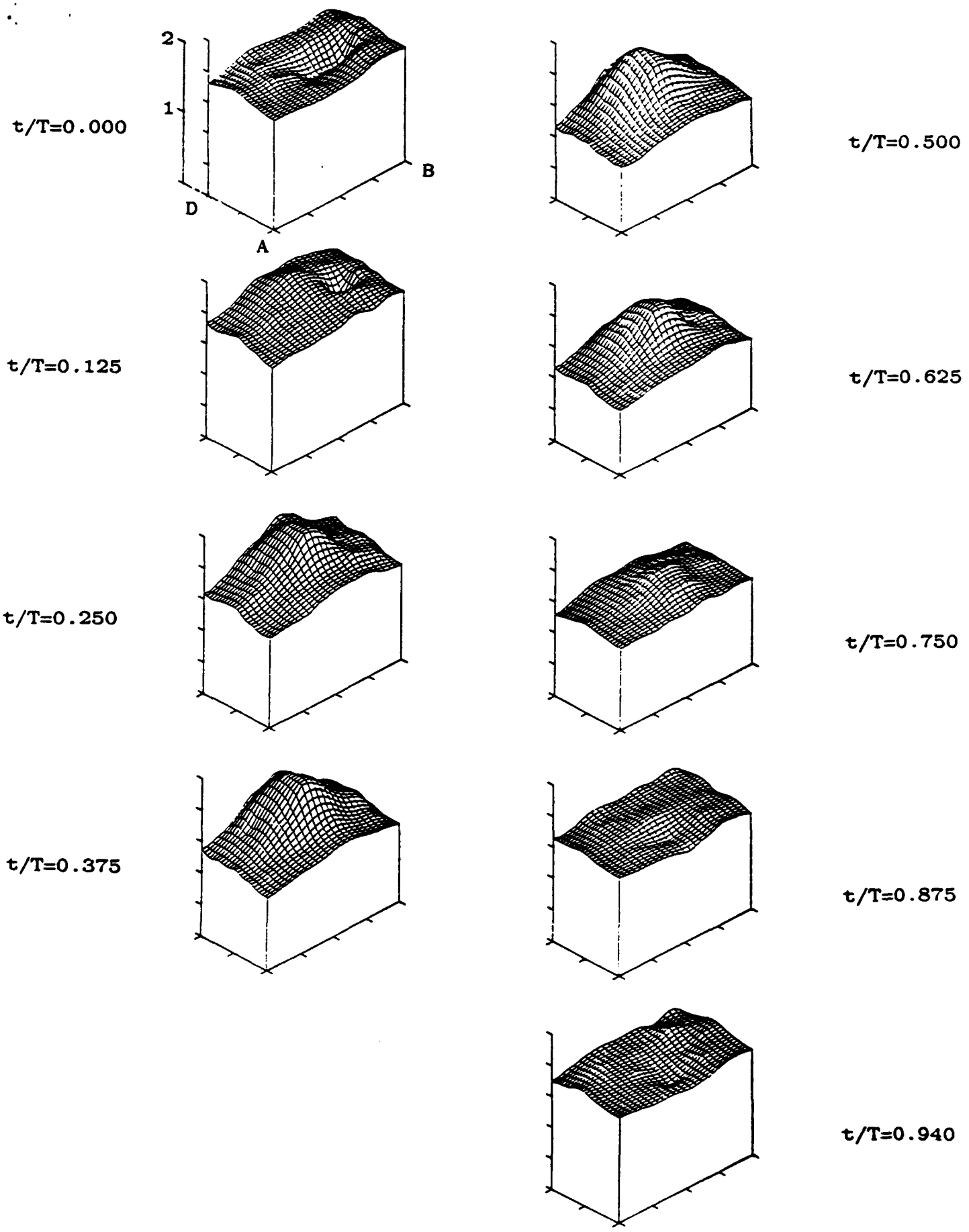

Figure 7: Axial velocity in cross plane at different phases of the cycle. α=15°, A=1, k=1.27, R=0.42 (as in figure 5).

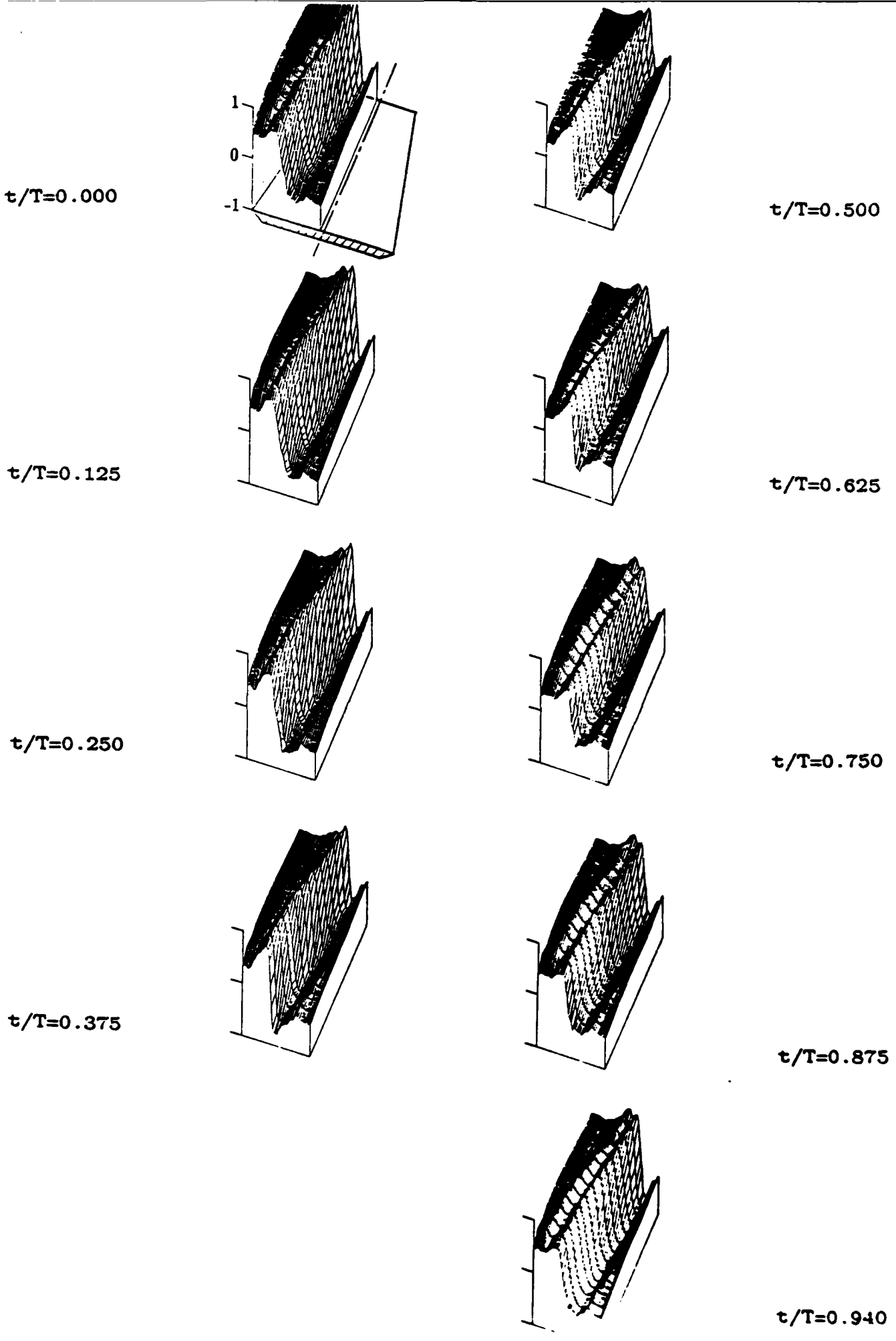

Figure 8: Swirl velocity across the core at different phases of the cycle, α=15°, A=1. k=1.27, R=0.42. (as in figure 5).

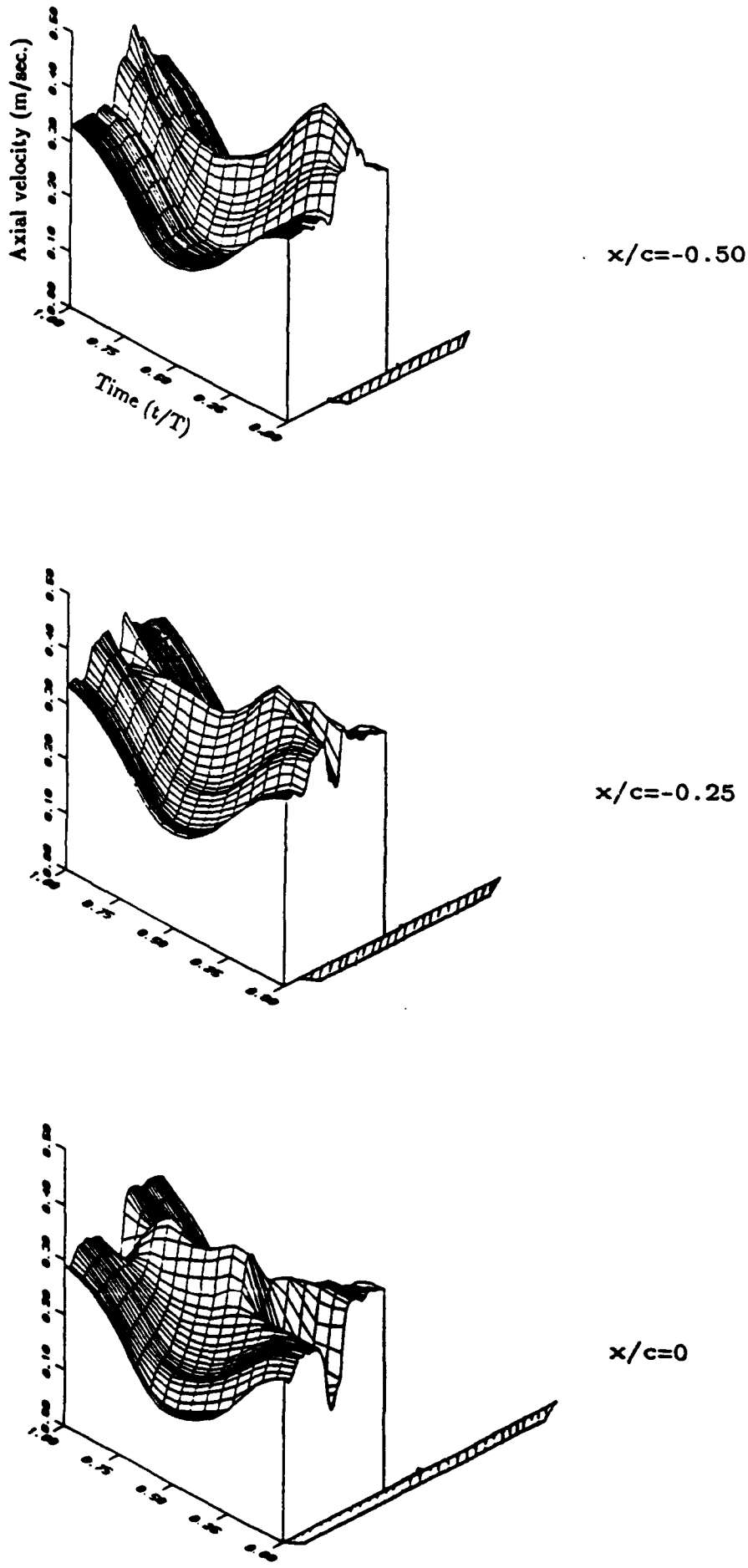

Figure 9: Time history of axial velocity across the core at different streamwise locations, α=15°, A=1, k=1.27, R=0.42 (as in figure 5).

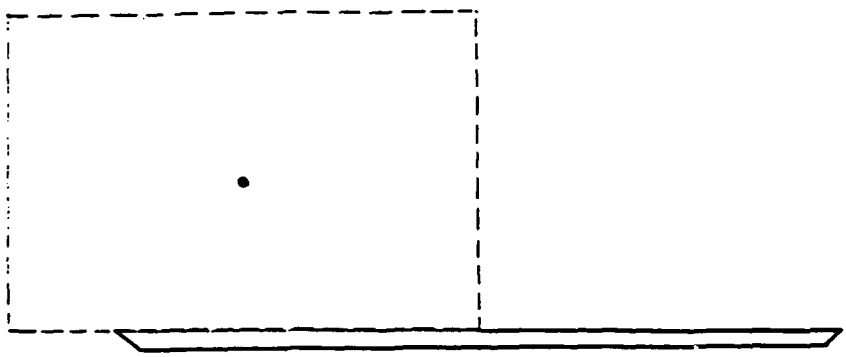

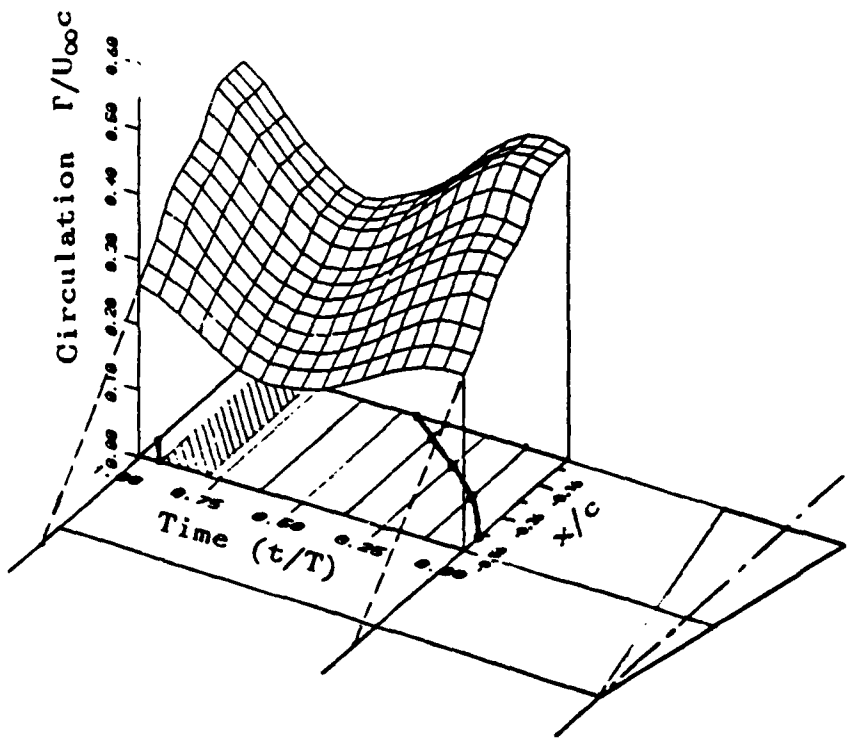

Figure 10: Path for circulation measurements and variation of dimensionless circulation as a function of streamwise distance and time, α=28°, A=1, k=1.27, R=0.42 (as in figure 4).

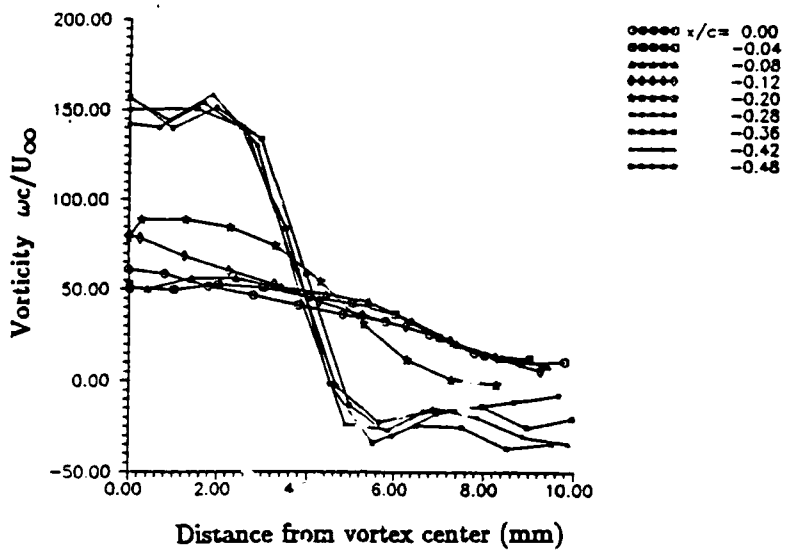

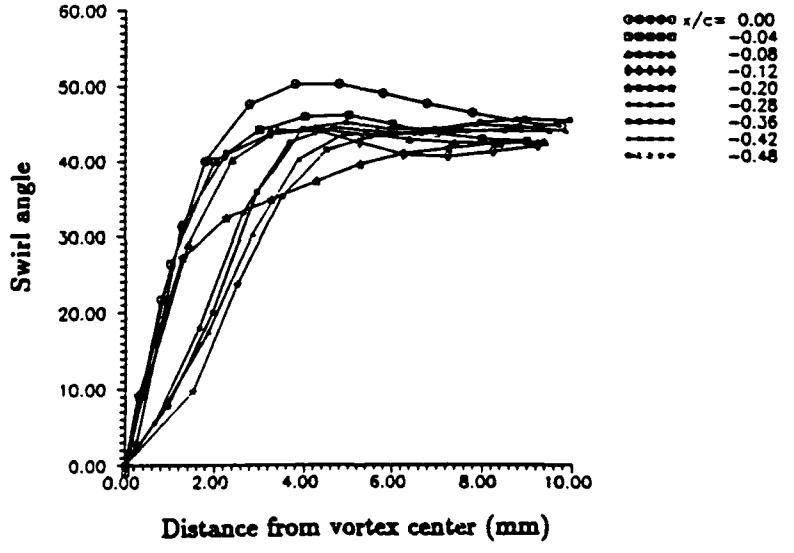

Figure 11: Vorticity (top) and swirl angle (bottom) as a function of distance from the vortex center at time t/T=0.125, α=28°, A=1, k=1.27, R=0.42 (as in figure 4).

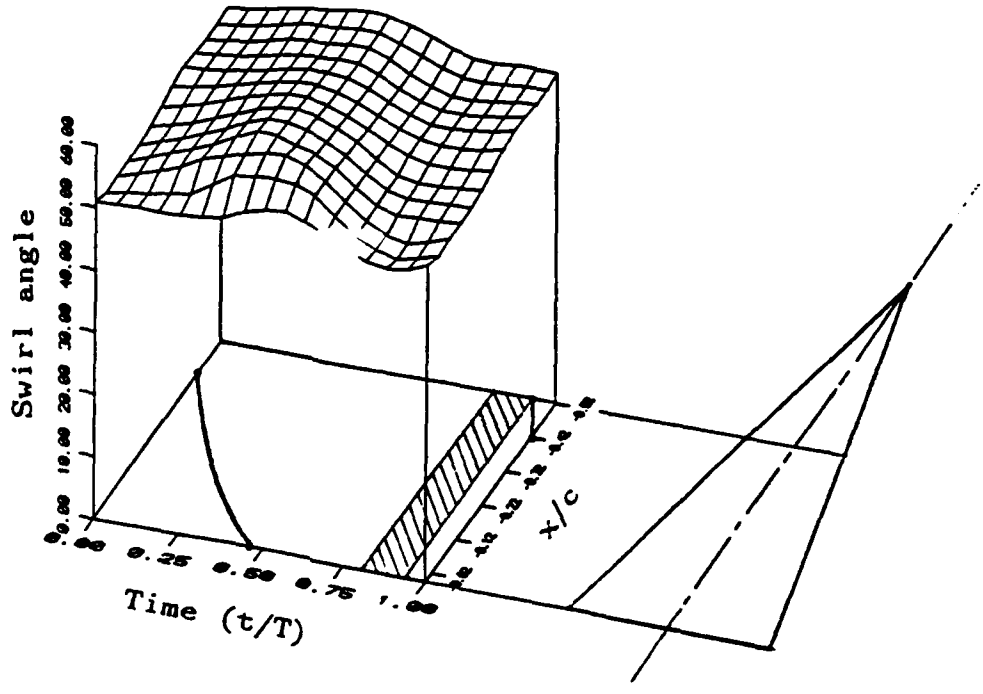

Figure 12: Variation of maximum swirl angle as a function of streamwise distance and time, α=28°, A=1, k=1.27, R=0.42 (as in figure 4).

VORTEX DYNAMICS OF DELTA WINGS IN UNSTEADY FREE STREAM

Ismet Gursul, Hank Lin and Chih-Ming Ho
Department of Aerospace Engineering
University of Southern California
Los Angeles, California 90089-1191

ABSTRACT

Response of several delta wings of varying aspect ratio in unsteady periodic free stream was investigated and compared to that of a 2-D wing. It was found that the characteristics of the lift forces depend on whether the leading-edge vortex sheds. For delta wings with attached leading-edge vortex, the lift forces are not a function of the reduced frequency, since there is no intrinsic time scale. At large angle of attack, the leading-edge vortices shed and convect downstream. Consequently, an intrinsic time scale appears and the lift force depends on the reduced frequency, which can be interpreted as the ratio of the convection time of the vortex on the chord to the period of the free stream variation. This type of behaviour is shown to be very similar to that of a 2-D wing in the poststall region.

INTRODUCTION

Unsteady aerodynamics of delta wings is very important for the development of highly maneuverable aircraft. Since the delta wings are being widely used in modern airplanes, their steady performance was investigated in extensive studies. However, their unsteady performance is not well known.

Unlike a 2-D wing, a delta wing can provide high lift coefficients even at very large angles of attack[1], up to 40°. This is due to a pair of stationary leading-edge vortices. The vorticity that originates from the leading edge is transported along the cores of the leading-edge separation vortices. The attached vortices make the delta wing behave very differently from a 2-D wing. With increasing angle of attack or aspect ratio, the vortex breakdown occurs on the wing and moves toward the apex. Vorticity transport along the core will be much reduced because of the vortex breakdown which has an abrupt change in axial velocity distribution from a jet-like axial velocity to a wake-like one. When the breakdown reaches the apex, delta wing behaves like a bluff body and vortex shedding occurs. If the breakdown is between the apex and trailing edge, the behaviour depends on the breakdown location

and aspect ratio. Vortex shedding type behaviour in the wakes of delta wings at high angle of attack was reported by Rediniotis et al[2]. In summary, there are two limiting cases (completely attached vortices and shed vortices) and the other operational conditions show transitional behaviour between the two.

The behaviour of leading-edge vortices in unsteady flows are not well understood. Some early experiments focused on a pitching delta wing[3] and a stationary delta wing in a vertical gust[4]. It was observed that the vortices may remain attached to the wing even in unsteady flows[3]. The three-dimensional development of vortex over a delta wing in a starting flow and over a pitching delta wing were was visualized by Freymuth[5]. It is very crucial to understand unsteady aerodynamics of delta wing for highly maneuverable aircraft.

In order to study the transition from delta wings to 2-D rectangular wings and understand the effects on unsteady aerodynamic loads, experiments on four airfoils were conducted. The three of these airfoils are delta wings with increasing aspect ratio A=1, 2 and 4; and the last one is a rectangular wing (NACA 0012). Obviously, the conditions which determine whether the vortices shed or not are related to vorticity dynamics. Vorticity is always generated at the leading edge and is convected into the outer flow for separated flows. The vorticity balance between the generation and convection will determine the global characteristics of the flow, thereby the aerodynamic forces. In this paper, the response of these wings in an unsteady free stream will be discussed with the aid of flow visualization, phase-averaged lift and velocity measurements. The effects of several geometrical and operational parameters will be discussed.

EXPERIMENTAL FACILITY

Experiments were conducted in a vertical unsteady water channel with a cross-sectional area of 45.7 by 45.7 cms. The flow between the top and bottom reservoirs is driven by gravitation and constant head operation eliminates nonlinear effects due to the pumps. The free stream control was achieved by rotating a gate (which operates like a valve) downstream of the test section. The rotation of the gate is done with a computer controlled stepping motor. The principle and process of controlling the free stream is explained in detail elsewhere[6]. This channel-gate combination provides a large range of amplitude and frequency of the time-varying free stream with different types of waveforms. Another important application is the transient experiments. For the oscillating free stream, the velocity can be represented in the form of:

$$U/U_{\infty} = 1+R\cos\omega t = 1+R\cos 2\pi t/T \qquad (1)$$

where U_{∞} is the average velocity, R is the dimensionless amplitude ($R<1$) and $\omega=2\pi/T$ is the

radial frequency. The frequency of the oscillations is limited by the fact that the free stream uniformity across the test section becomes unacceptable for $\omega \geq 6$ sec^{-1}. This is because of the flow separation in the contraction section due the unsteadiness. The free stream turbulence level was about 0.5%. The free stream velocity was measured with a two-component Laser Doppler Anemometer (LDA) (DANTEC, 55X optical system) operated in forward-scattering mode and equipped with a 100 mW Argon-Ion laser (Ion Laser Technology) and LDA counters (DANTEC 55L96).

The delta wings are made of thin plates with sharp leading-edges. The NACA 0012 airfoil was cast from Hysol mixture. The Reynolds number was in the range of 30,000 to 60,000 for all airfoils. The blockage ratio was 0.135 for the rectangular wing at the maximum angle of attack α=30° and 0.044 for the delta wings at the maximum angle of attack α=40°. No correction was made on lift measurements due to the blockage. A pair of waterproof load cells (Sensotec, model 31) were used to measure the lift force on airfoils. Lift and velocity signals were digitized by an analog-to-digital converter (RC Electronics, model ISC-67) and processed by an UNIPAQ 386 personal computer. Ensemble-averaging technique was applied to the signals to extract deterministic parts. An average of 50 cycles with 100 points per cycle were averaged.

The phase-averaged lift force and lift coefficient are defined by:

$$L(t) = C_L(t) \frac{1}{2} S \rho U(t)^2 \qquad (2)$$

where S is the surface area of the wing. In order to see effects of unsteadiness, a comparison is made with the *quasi-steady* lift force defined as:

$$L_{qs}(t) = C_{L_\infty} \frac{1}{2} S \rho U(t)^2 \qquad (3)$$

where C_{L_∞} is the steady-state lift coefficient. Then, the ratio of the time-averaged values of these forces is considered, i.e.

$$\overline{L(t)} / \overline{L_{qs}} \qquad (4)$$

Flow visualization was carried out by illuminating air bubbles which were entrained into the vortex vores on delta wings, providing a way to visualize leading-edge vortices. A tungsten light source made of two 500 W lamps with a slit as well as a laser sheet scanned by a mirror was used to illuminate the flow field. A 35 mm camera (NIKON, model F-2) was used in taking still pictures. This camera could be triggered by a pulse at any particular time which is phase-referenced to the pulse train used for the rotating gate. The time-dependent flow field was also videotaped using a CCD camera (ELMO, model SE301) and a VCR (Panasonic S-VHS). In order to provide a reference, a LED

indicator was used.

RESULTS

Two important time scales exist when an airfoil is placed in an unsteady free stream: an intrinsic vortex convection time scale c/U_∞ (c is the chord length) and external perturbation time scale $T=2\pi/\omega$. The convective time scale c/U_∞ can be considered as a measure of the time needed for a vortex to pass the airfoil. This physical interpretation is meaningful when a vortex shedding from the leading-edge takes place. Then, the reduced frequency $k=\omega c/2U_\infty$ can be interpreted as the ratio of these time scales. Effect of the reduced frequency on aerodynamic load was studied for different wings.

The time-averaged lift force normalized as in (4) is shown as a function of the reduced frequency in figures 1-4 for all wings. The solid and open symbols denote different amplitudes of oscillations ($R\approx0.42$ and $R\approx0.59$). Note that, for the smallest aspect ratio delta wing (A=1, in figure 1), the time-averaged lift force is not a function of the reduced frequency for a large range of angles of attack. In figure 5, the flow visualization at $\alpha=25^\circ$ (at a relatively high reduced frequency, k=0.93) is shown at different stages of the cycle. It is seen that the vortex core remains attached to the wing and essentially in the same position with respect to the wing. In other words, the geometry of the core does not change. Since the vortices remain attached, there is no intrinsic time scale. Therefore, the reduced frequency is not a controlling parameter.

Further flow visualization showed that while the breakdown may be in the wake at all times for low reduced frequencies, it is observed around the trailing edge (and on the wing) during a portion of the cycle for high reduced frequencies. However, the time-averaged lift force does not change with the reduced frequency (see figure 1). This implies that the observed changes in the breakdown position near the trailing-edge does not really affect the lift force. This is not surprising because of the Kutta condition which requires vanishing pressure difference between the upper and lower surfaces as the trailing-edge is approached. This has been demonstrated by pressure measurements in the steady case by Lambourne and Bryer[7]. In addition, they demonstrated that pressure undergoes very gradual change with the vortex burst.

At the largest angle of attack ($\alpha=40^\circ$), a departure in the time-averaged lift force seems to begin. The vortex breakdown position is approximately at mid-chord for this angle of attack. In figure 6, the flow visualization is shown at the same reduced frequency as in figure 5. In this case, the breakdown does not seem to be affected by unsteadiness in free stream. In general, the breakdown is not sensitive to the unsteadiness, except when it is near the trailing-edge.

Unlike the A=1 delta wing, the time-averaged lift force is a strong function of the reduced

frequency for the 2-D wing in the poststall region (figure 4). This is because the intrinsic vortex convection time scale plays an important role. However, when the flow is attached for small angle of attack (α=5°), there is no convected vortex, and the lift is not a function of the reduced frequency anymore.

The response of delta wings at aspect ratios higher than one has transitional behaviour between the 2-D wing and A=1 delta wing. When the aspect ratio or angle of attack is increased, the convection of vorticity along the cores of the leading-edge vortices in the streamwise direction decreases. As the accumulated vorticity increases, the leading-edge vortices start shedding. In this case, the intrinsic convection time scale appears on the delta wing. The lift force depends on the reduced frequency just like it does for the 2-D wing. In figure 7, flow visualization for A=4 delta wing, at α=40°, is shown at different phases of the cycle. There are strong similarities to the flow around a rectangular wing in the poststall region[8].

So far discussion was based on the time-averaged lift force. However, the same conclusions can be arrived by studying phase-averaged lift coefficient. In order to make a comparison of the phase-averaged lift coefficient, the results at α=30° for all airfoils are presented in figures 8-11. It is seen that when the leading-edge vortices are attached (A=1), the phase-averaged lift coefficient is not a function of the reduced frequency and all the curves collapse for a given amplitude. However, for large angle of attack or large aspect ratio, vortex convection becomes important. Consequently, the reduced frequency is an important parameter and lift coefficient curves do not collapse.

With increasing aspect ratio, vortex shedding and lift force variation become more similar to that of the rectangular wing. However, the maximum values of the lift coefficient for the rectangular wing are much higher. In fact, the NACA 0012 airfoil in the poststall region can have lift coefficients exceeding 10 at an optimum reduced frequency[8]. This is because a large coherent vortex is trapped on the chord for an appreciable portion of the cycle.

CONCLUSIONS

Response of vortical flows has been investigated in an unsteady free steam. The time-averaged and phase-averaged lift measurements show that the reduced frequency is not a controlling parameter if the leading-edge vortices are attached. This occurs for delta wings with small angle of attack or aspect ratio. With increasing angle of attack or aspect ratio, vortex shedding can occur, and the time required to convect along the chord becomes an intrinsic time scale. Hence, the lift is a function of the reduced frequency. In the limiting case, for the poststall region of the rectangular wing, the time-averaged lift force and phase-averaged lift coefficient can reach very high values compared to steady case.

When the reduced frequency reaches relatively high values ($k \approx 1$), the breakdown may be

influenced by the unsteady free stream depending on its location. When the breakdown is in the wake and around the trailing-edge, it was found to be sensitive to unsteadiness in the free stream. This sensitivity decreases quickly as the steady state location approaches the apex. (The breakdown was observed to be not influenced, if it is located 50-60% of the chord length from the apex). This is also true for steady free stream; the burst position is very sensitive to external perturbations (for example, to angle of attack[7] or leading edge shape[9]) when it is around the trailing-edge. However, the surface pressure does not seem to be influenced by the vortex breakdown[7,10]. These results together with the Kutta condition explain the fact that the aerodynamic forces are not affected by vortex breakdown. However, it is possible that the breakdown might be important for low aspect ratio wings. Because the contribution of leading edge vortex to lift force mainly depends on the aspect ratio[1] according to the Polhamus's leading-edge suction analogy, which suggests that "vortex lift" contribution increases with decreasing aspect ratio.

ACKNOWLEDGEMENT

This work is supported by AFOSR Contract No. F49620-88-C-0061.
90-C-0058

REFERENCES

1. Lee, M. and Ho. C.M., "Lift force of delta wings", *Applied Mechanics Reviews*, vol. 43, no.9, September 1990, pp. 209-221.

2. Rediniotis, O.K., Stapountzis, H. and Telionis, D.P., "Vortex shedding over delta wings", *AIAA Journal*, vol. 28, no. 5, 1990, pp. 944-946.

3. Gad-el-Hak, M. and Ho., C.M., "The pitching delta wing", *AIAA Journal*, vol. 23, no. 11, 1985, pp. 1160-1665.

4. Patel, M.H. "The delta wing in oscillatory gusts", *AIAA Journal*, vol. 18, no. 5, May 1980, pp. 481-486.

5. Freymuth, P. "Air flow visualization using titanium tetrachloride", Lecture Notes in Engineering, vol 45, Springer-Verlag, pp. 1-31, 1989.

6. Gursul, I., Lin, H. and Ho, C.M., "Vorticity dynamics of 2-D and 3-D wings in unsteady free stream", AIAA Paper 91-0010, January 1991.

7. Lambourne, N.C. and Bryer, D.W., "The bursting of leading-edge vortices-Some observations and discussions of the phenomena", Aeronautical Research Council, R&M. No. 3282, 1961.

8. Gursul, I. and Ho, C.M., "High aerodynamic loads on an airfoil submerged in an unsteady stream", (submitted to *AIAA Journal*), 1991.

9. Panton, R.L. "Effects of a contoured apex on vortex breakdown", *Journal of Aircraft*, vol. 27, no. 3, 1990, pp. 285-288.

10. Thompson, S., Batill, S. and Nelson, R., "Unsteady surface pressure distributions on a delta wing undergoing large amplitude pitching motions", AIAA-90-0311, January 1990.

LIST OF FIGURES

Figure 8: Variation of phase-averaged lift coefficient normalized by the steady one, $C_L/C_{L\infty}$, for aspect ratio A=1, α=30°.

Figure 9: Variation of phase-averaged lift coefficient normalized by the steady one, $C_L/C_{L\infty}$, for aspect ratio A=2, α=30°.

Figure 10: Variation of phase-averaged lift coefficient normalized by the steady one, $C_L/C_{L\infty}$, for aspect ratio A=4, α=30°.

Figure 11: Variation of phase-averaged lift coefficient normalized by the steady one, $C_L/C_{L\infty}$, for rectangular wing, α=30°.

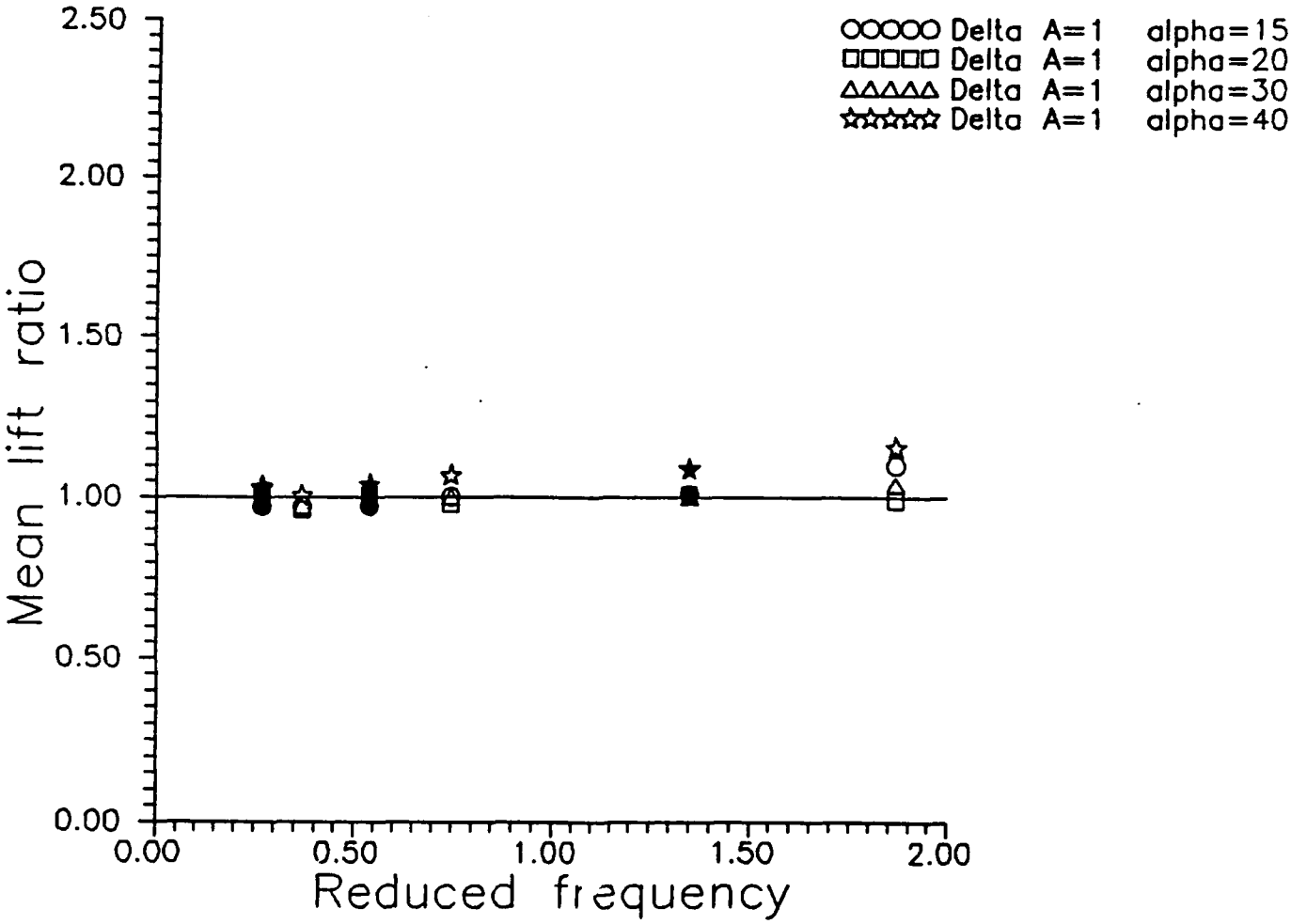

Figure 1: Variation of time-averaged lift force normalized by time-averaged quasi-steady lift force for aspect ratio A=1.

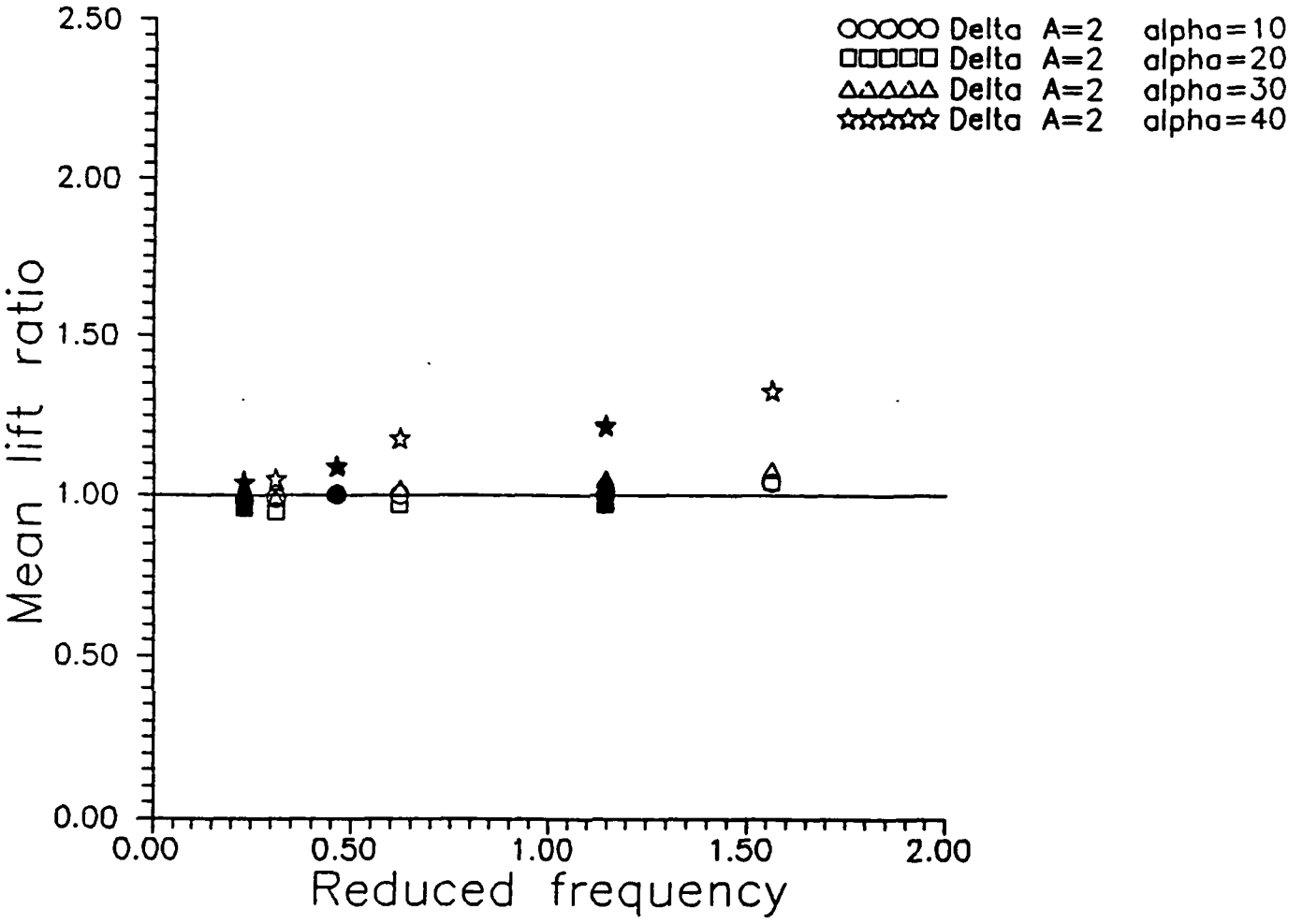

Figure 2: Variation of time-averaged lift force normalized by time-averaged quasi-steady lift force for aspect ratio A=2.

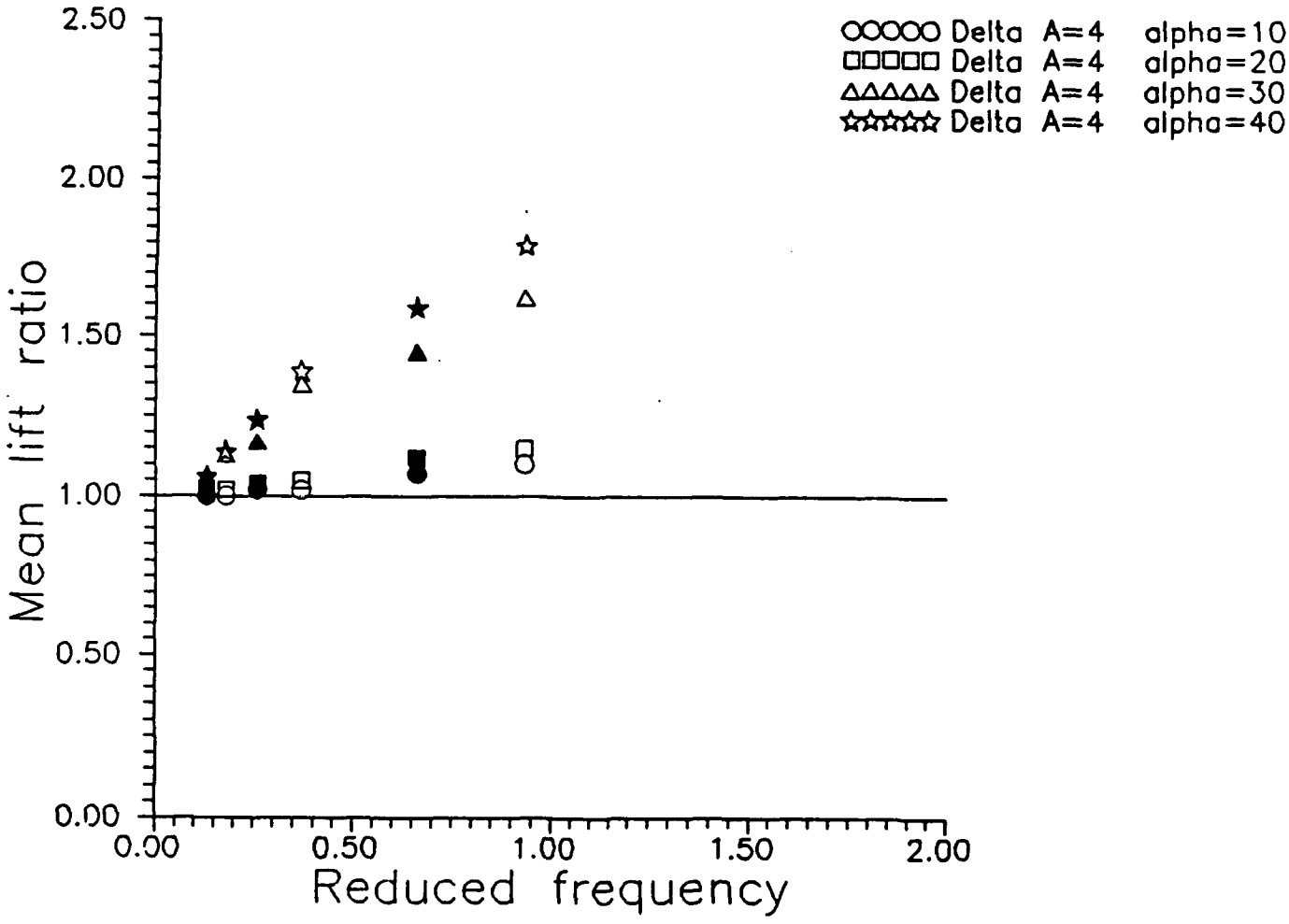

Figure 3: Variation of time-averaged lift force normalized by time-averaged quasi-steady lift force for aspect ratio A=4.

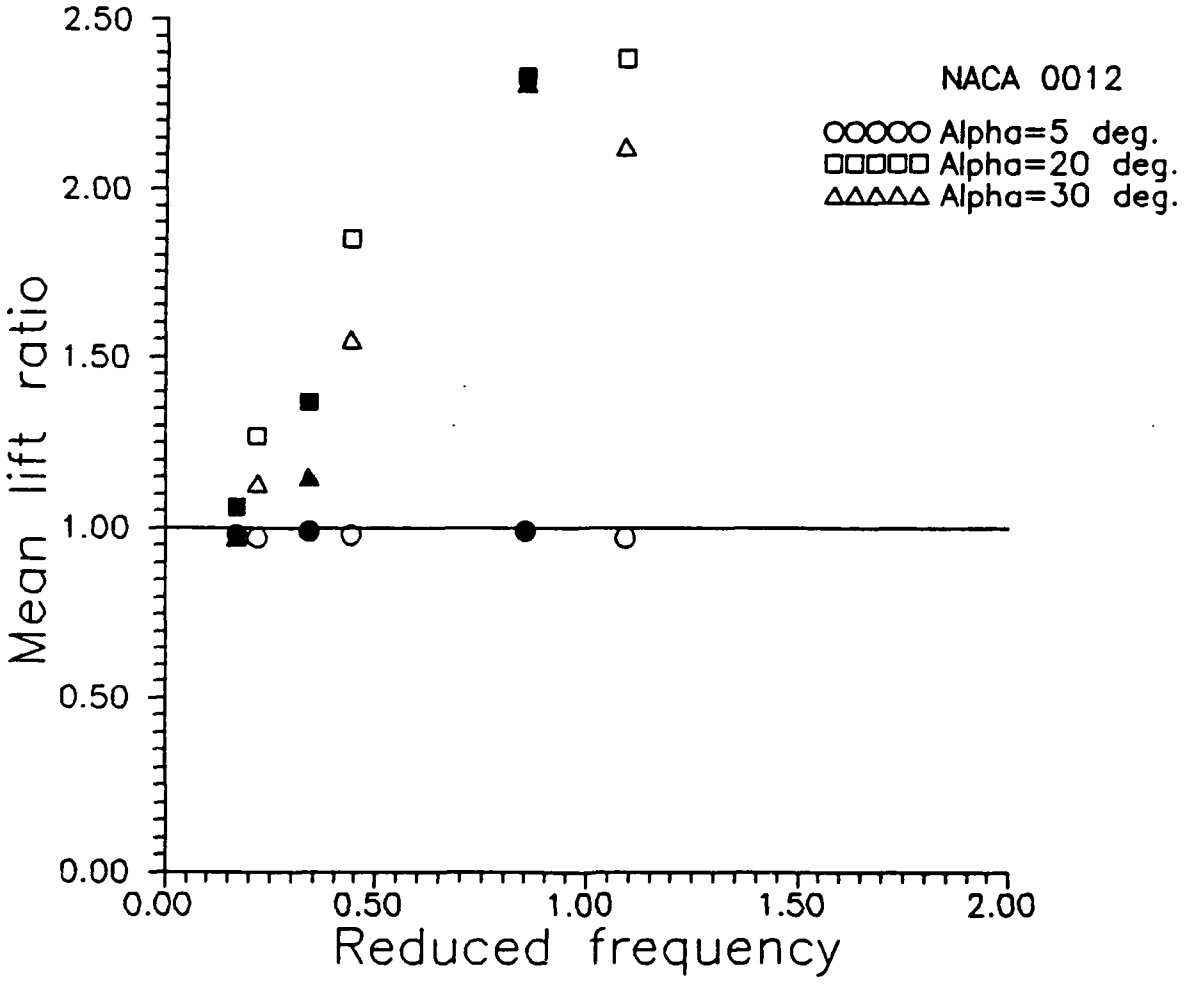

Figure 4: Variation of time-averaged lift force normalized by time-averaged quasi-steady lift force for rectangular wing.

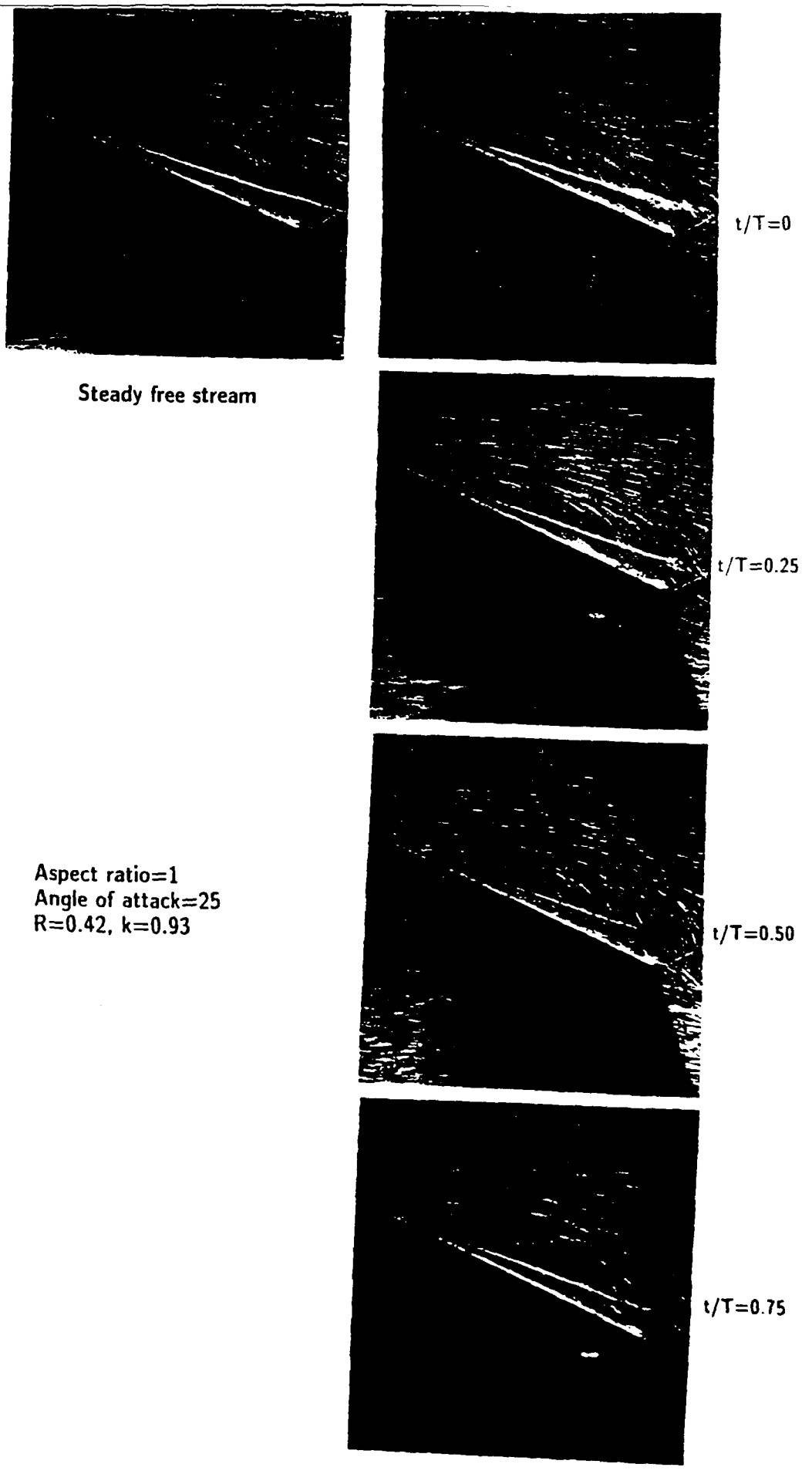

Figure 5: Flow visualization for A=1 delta wing at α=25° at different phases of the cycle (k=0.93, R=0.42).

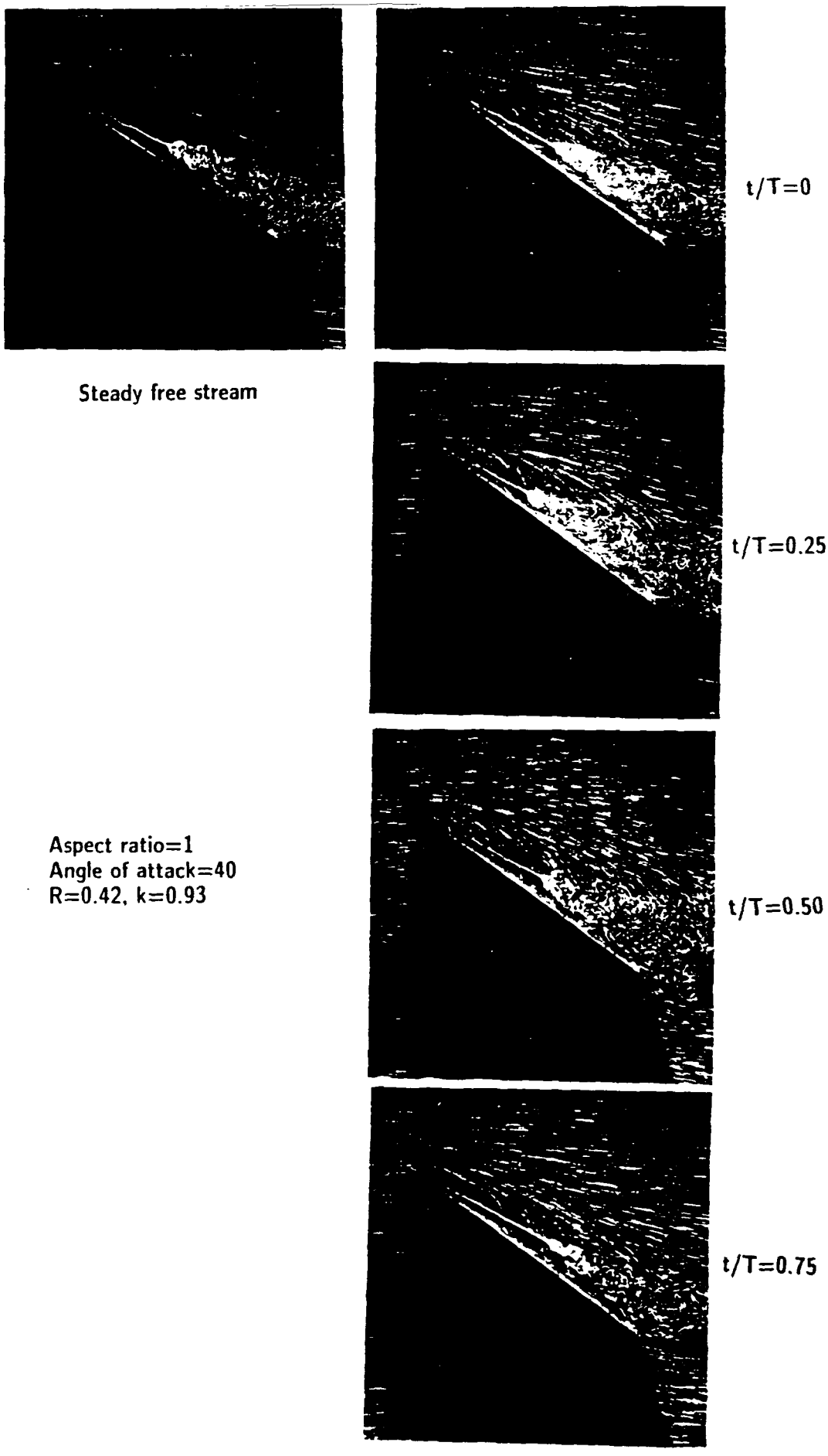

Figure 6: Flow visualization for A=1 delta wing at $\alpha=40^{\circ}$ at different phases of the cycle (k=0.93, R=0.42).

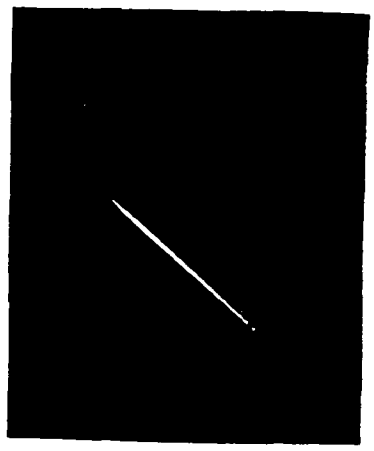

Steady free stream

t/T=0

t/T=0.25

t/T=0.50

Aspect ratio=4
Angle of attack=40
R=0.70, k=0.93

t/T=0.75

Figure 7: Flow visualization for A=4 delta wing at $\alpha=40^{\circ}$ at different phases of the cycle (k=0.93, R=0.70).

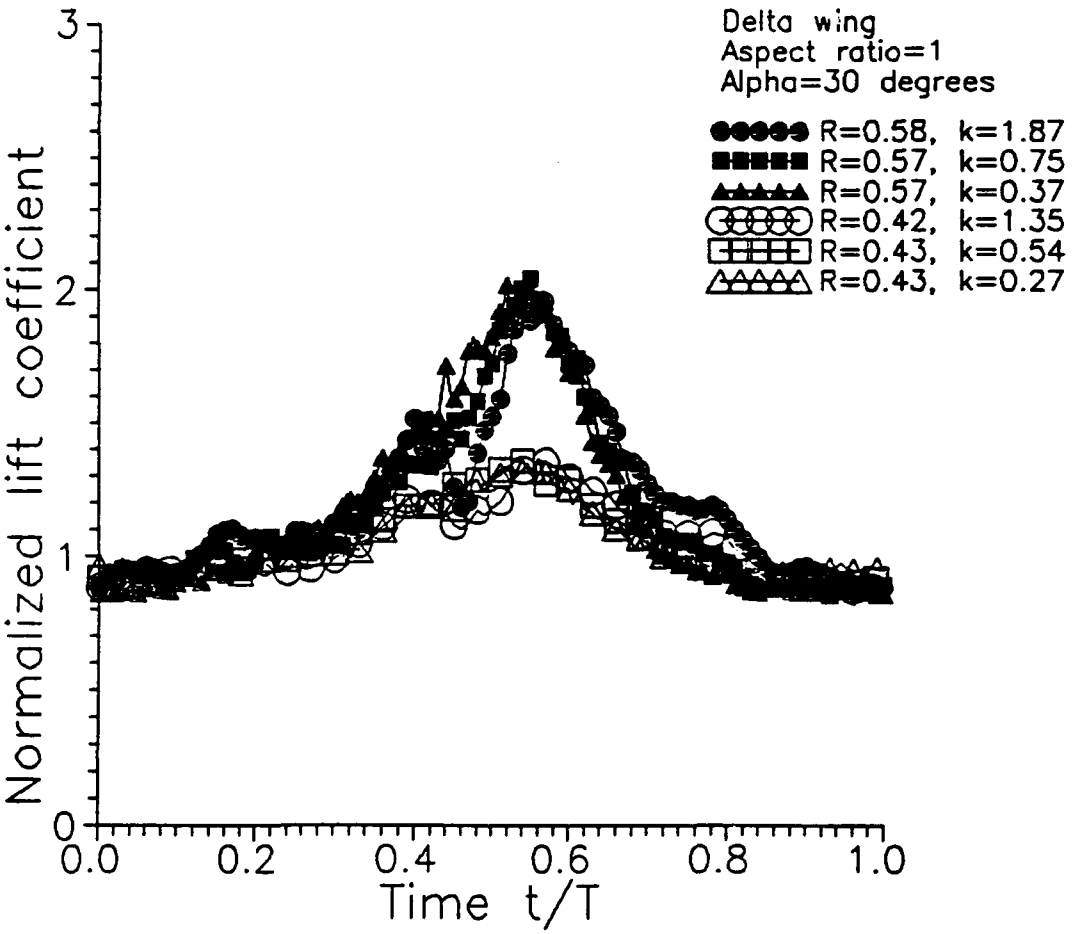

Figure 8: Variation of phase-averaged lift coefficient normalized by the steady one, $C_L/C_{L\infty}$, for aspect ratio A=1, α=30°.

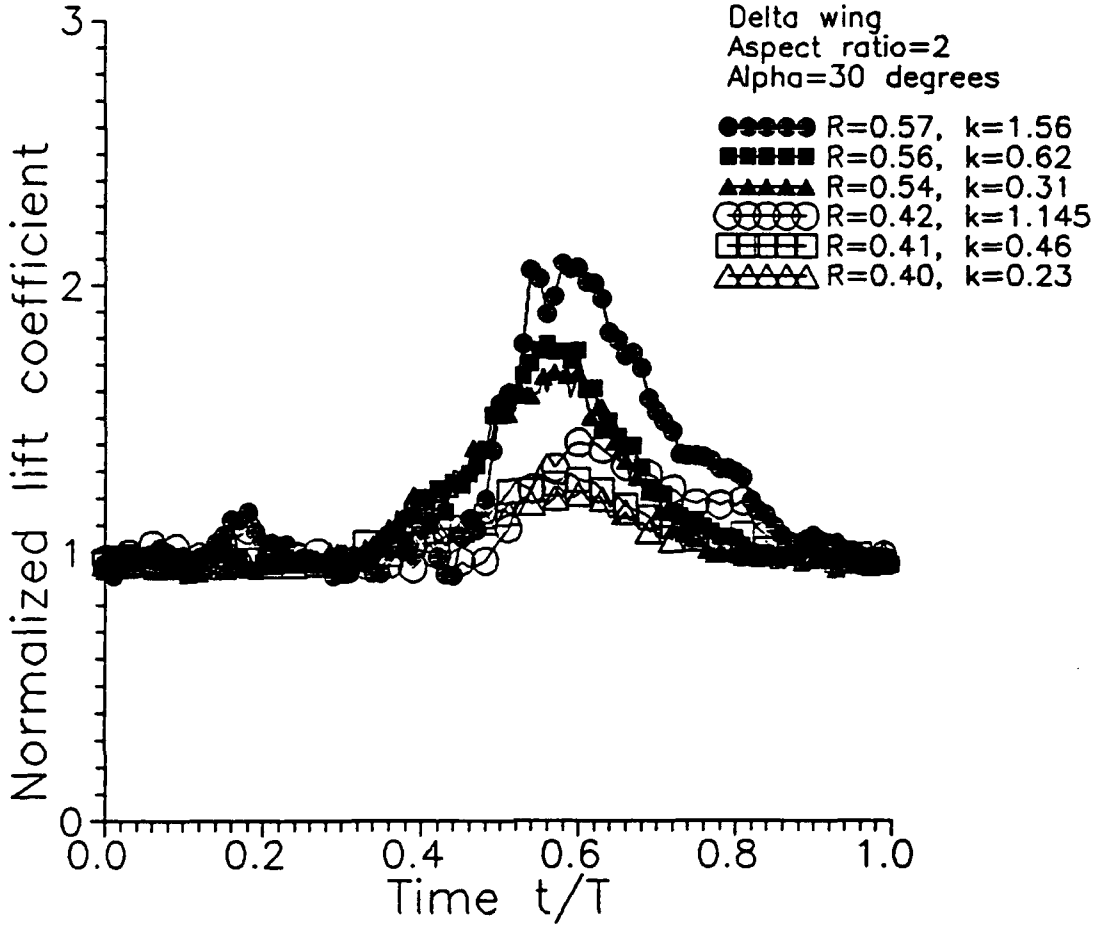

Figure 9: Variation of phase-averaged lift coefficient normalized by the steady one, $C_L/C_{L\infty}$, for aspect ratio A=2, α=30°.

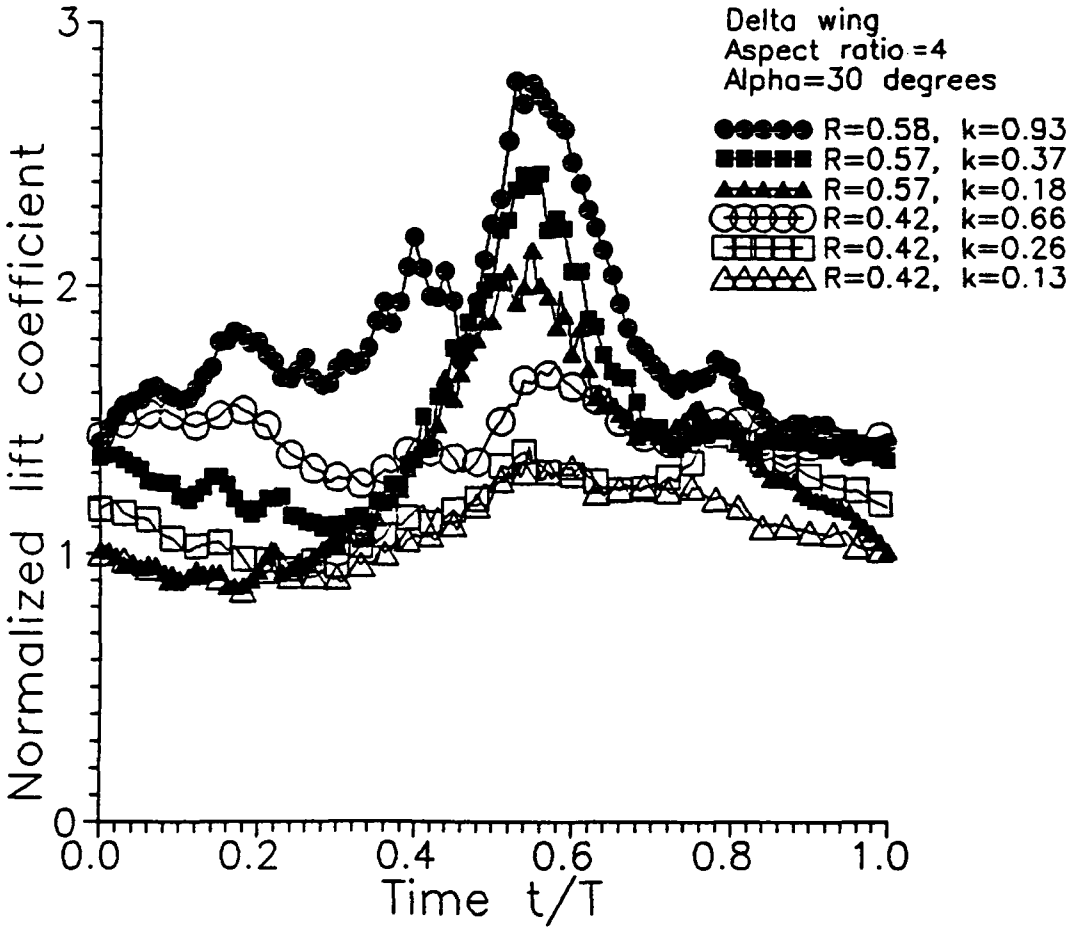

Figure 10: Variation of phase-averaged lift coefficient normalized by the steady one, $C_L/C_{L\infty}$, for aspect ratio A=4, α=30°.

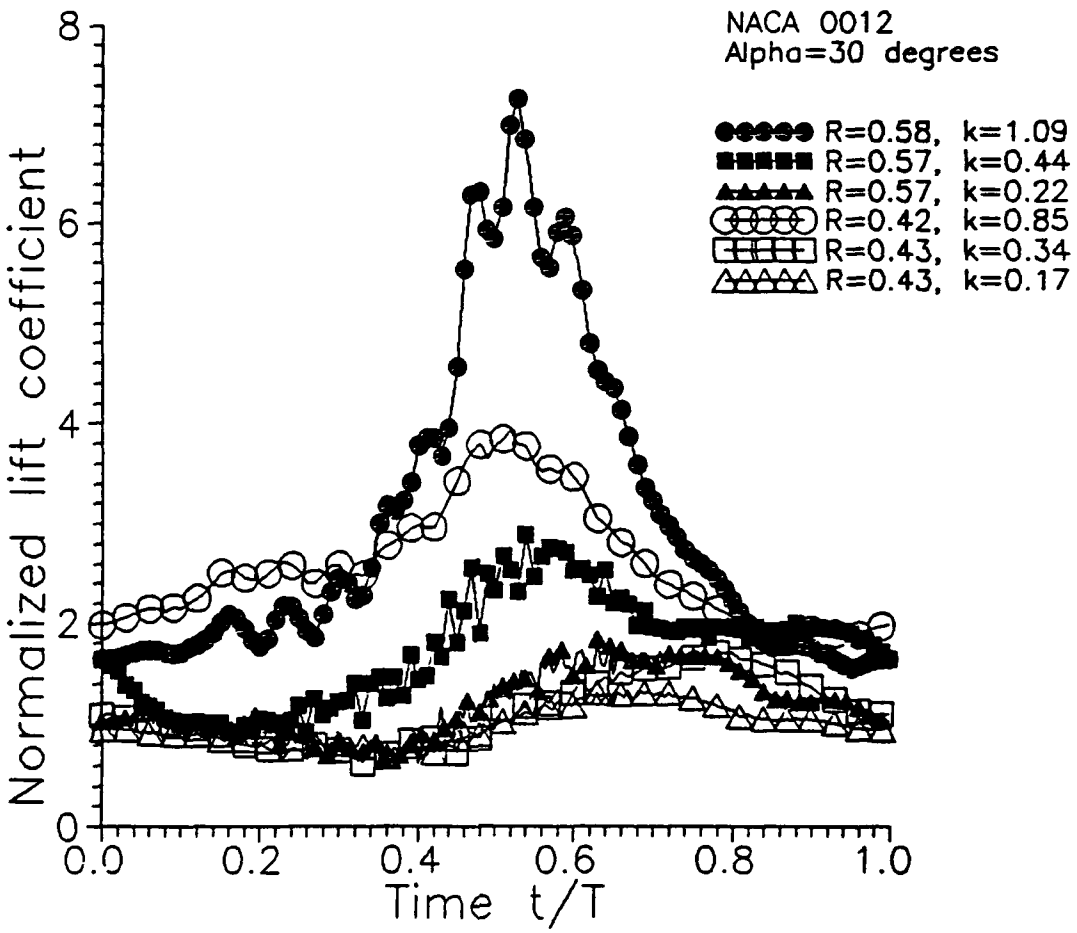

Figure 11: Variation of phase-averaged lift coefficient normalized by the steady one, $C_L/C_{L\infty}$, for rectangular wing, α=30°.

VORTEX DYNAMICS OF SEPARATED FLOW OVER AN AIRFOIL IN UNSTEADY FREE STREAM

Ismet Gursul, Hank Lin and Chih-Ming Ho
Department of Aerospace Engineering
University of Southern California
Los Angeles, California 90089-1191

ABSTRACT

Response of a rectangular airfoil in unsteady free stream was investigated in a unsteady water channel. It is shown that, in the poststall region, the time-averaged and phase-averaged lift force is a strong function of the reduced frequency which is the ratio of convective time scale to the free stream period. This is due to the vortex shedding from the leading-edge and is in contrast to attached flows such as slender delta wings or small angle of attack flows for which vortex shedding does not occur. There is an optimum reduced frequency at which the time-averaged lift force becomes maximum. Very high lift coefficients exceeding 10 can be observed at the optimum reduced frequency which is very much independent from amplitude and angle of attack. This high aerodynamic loads are due to a large coherent vortex which sheds from the leading-edge and stays on the wing for an appreciable portion of the cycle.

INTRODUCTION

Many flows in nature and technology involve cases where the free stream velocity is time-dependent. An aircraft undergoing maneuver is the simplest case. During the forward flight of a helicopter, the free stream velocity varies periodically accompanied by variations in angle of attack. Other examples are rotary wing aircrafts and turbomachines. Many birds are known to have large backward and forward wing stroke superimposed on up-and-down strokes as they fly forward[1]. One of the purposes of this study is to understand the response of lifting surfaces in unsteady free stream.

Recent interest in highly maneuverable aircraft motivated research in understanding unsteady separation and control of separated flows. For an airfoil in steady free stream, the flow is separated at the leading-edge at an angle of attack larger than the static stall angle. The vorticity shed from the leading-edge is disorganized and the lift force experiences a decrease. However, when the separation is forced by external perturbation, the shear layer vorticity lumps into a vortex. This vortex can greatly alter the surface loading as it is convected by the mean flow[2,3]. Based on the vorticity balance

concept[4], Shih[5] demonstrated that the aerodynamic properties are determined by the rate of the depletion and accumulation of the vorticity on the chord. Understanding the relationship between lift development and vorticity balance may lead to better control of aerodynamic performance.

The "vortex lift" can be used in supermaneuverable aircraft for which high lift coefficients in the poststall region is important. The idea of taking advantage of leading edge vortices to increase the lift on a large-aspect-ratio airfoil was suggested by Kasper.[6] Steady two-dimensional potential flow over a wing with an attached free vortex was calculated by Saffman and Sheffield.[7] It was found that the convex streamlines provide large suction which creates a high lift coefficient for the wing. However, the leading edge vortex usually cannot stay on the wing and will shed, leading to loss of high lift.

In this study, particular attention is given to large angle of attack flow over a rectangular airfoil. For periodically varying free stream, the amplitude and frequency were varied over a large range. Velocity and lift measurements were carried out and interpreted with the help of flow visualization. The results show that time-averaged and phase-averaged performance can be enhanced and becomes maximum at an optimum reduced frequency. Therefore, this might be an effective way of taking advantage of leading-edge vortices in the post-stall region.

EXPERIMENTAL FACILITY

Water channel and free stream control

Experiments were conducted in a vertical unsteady water channel with cross-sectional area of 45.7x45.7 cms (figure 1). The flow between the top and bottom reservoirs is driven by gravity and constant head operation eliminates nonlinear effects due to the pumps. During the operation, a net head of 3.7 m exists between the top and bottom reservoirs. The bottom section of the facility consists of a rotating gate and a stationary gate which have identical opening patterns. The velocity in the test section varies as the relative angular displacement between the gates is varied by a computer-controlled stepping motor. The principle and procedure of obtaining a desired free stream variation are explained in detail elsewhere[8]. The basic idea is to rotate the gate at a variable angular speed such that the desired velocity variation is obtained. The pulse trains corresponding to 2,000 steps per revolution of the stepping motor were calculated with this method and sent by a Personal Computer to a system consisted of the stepping motor (SLO-SYN, model MH172-FD-8030), the driver (MODULYNX, model DRD004), and the microstep translator card (MODULYNX, model MID014).

A third gate above the stationary gate (not shown in figure 1) allows to vary amplitude of

velocity oscillations. In summary, this channel-gate combination provides a large range of amplitude and frequency of the time-dependent free stream with different types of waveforms. Another important application is the transient experiments. For the oscillating free stream, the velocity can be represented in the form of:

$$U/U_\infty = 1+R\cos\omega t = 1+R\cos 2\pi t/T \qquad (1)$$

where U_∞ is the average velocity, R is the dimensionless amplitude ($R<1$) and $\omega=2\pi/T$ is the radial frequency. Examples of free stream variation are presented by Gursul et al[8]. The free stream has been found to be uniform across the test section during the whole cycle as long as $\omega \leq 6$ sec^{-1}. This limit corresponds to the highest frequency below which no boundary layer separation takes place in the contraction section due to free stream unsteadiness. The free stream turbulence was about 0.5%.

Instrumentation and Techniques

The velocity filed was measured with a two-component Laser Doppler Anemometer (LDA) (DANTEC, 55X optical system) operated in forward-scattering mode and equipped with a 100 mW Argon-Ion laser (Ion Laser Technology) and two LDA counters (DANTEC 55L96). The optical system was equipped with a beam expander and bragg cell for frequency shifting in reversed flows. The nominal measuring volume was estimated to be about 0.2 mm in diameter and 4 mm in length.

The NACA 0012 airfoil (with chord length c=12.4 cm) was cast from Hysol mixture. The Reynolds number based on the maximum free stream velocity was in the range of 30,000 to 60,000. The blockage ratio was 0.089 for $\alpha=20^\circ$ for which most of the experiments were carried out. Some lift measurements at $\alpha=30^\circ$ was also made (blockage ratio 0.135). No blockage correction was made for the lift measurements. A pair of waterproof load cells (Sensotec, model 31) were used to measure the lift force on the airfoil which spans the whole cross-section of the tunnel with a small gap of 3 mm near the wall. The load cells were mounted with their sensitive axis in the horizontal direction in two enclosed boxes filled with water. The measurement system was found very insensitive to drag, which was tested by hanging weights vertically. An estimate of the error due to the drag component is 0.5%.

Lift and velocity signals were digitized by an analog-to-digital converter (RC Electronics, model ISC-67) and processed by an UNIPAQ 386 personal computer. Ensemble-averaging technique was applied to the signals to extract deterministic parts. An average of 50 cycles with 100 points per cycle were averaged.

The phase-averaged lift force and lift coefficient are defined by:

$$L(t) = C_L(t)\,\tfrac{1}{2}\,S\,\rho\,U(t)^2 \qquad (2)$$

where S is the surface area of the wing. The effect of the unsteadiness on the overall performance is best illustrated by considering the average force. For this purpose, a comparison is made with the time-averaged *quasi-steady* lift force, i.e.

$$\overline{L(t)}/\ \overline{L_{qs}} \tag{3}$$

The quasi-steady lift force is defined as:

$$L_{qs}(t) = C_{L_\infty}\ \tfrac{1}{2}\ S\ \rho\ U(t)^2 \tag{4}$$

where C_{L_∞} is the steady-state lift coefficient. The main reson for the introduction of the quasi-steady force is that it allows to isolate the effects of the unsteadiness only and make a comparison between the experiments for different amplitude R. This is due to the fact the time-averaged free stream dynamic preesure is dependent on the amplitude, i.e. $\overline{U(t)^2}=(1+R^2/2)\ U_\infty{}^2$.

Flow visualization was carried out by illuminating air bubbles by a thin light sheet. A vacuum pump which is normally used to remove the air bubbles from the top of the channel was shut off during the flow visualization in order to provide more bubbles as flow tracers. A tungsten light source made of two 500 W lamps with a slit as well as a laser sheet scanned by a mirror was used to illuminate the flow field. A 35 mm camera (NIKON, model F-2) was used in taking still pictures. This camera could be triggered by a pulse at any particular time which is phase-referenced to the pulse train used for the rotating gate. The time-dependent flow field was also videoaped using a CCD camera (ELMO, model SE301) and a VCR (Panasonic S-VHS). In order to provide a reference, a LED indicator was used. An example of instantaneous picture of the flow field at angle of attack $\alpha=20^\circ$ in steady free stream is shown in figure 2. The lift coefficient in the range of Reynolds number Re=30,000-60,000 is around 0.8.

RESULTS

1. *Effect of time scales and an optimum reduced frequency*

Two important time scales in this unsteady flow are: convective time scale c/U_∞ (c is the chord length) and external perturbation time scale $T=2\pi/\omega$. The convective time scale c/U_∞ is a measure of the time needed for a vortex to pass the airfoil. The reduced frequency $k=\omega c/2U_\infty$ can be interpreted as the ratio of these time scales. Of course, this physical interpretation is meaningful when

a vortex shedding from the leading-edge takes place. It is expected that the aerodynamic forces will be a strong function of the reduced frequency whenever vortex shedding occurs. (This is in contrast to the response of slender delta wings where the leading-edge vortices remain attached and the lift force is not a function of the reduced frequency[8]).

The time-averaged lift force normalized as in (3) is shown as a function of the reduced frequency in figure 3 for α=20°. This ratio increases with increasing amplitude R. At the largest amplitude R=0.7, the maximum value is close to three. Note that there is an optimum reduced frequency at which the time-averaged lift force becomes maximum. The optimum reduced frequency does not depend on the velocity amplitude R and has a value of around 0.8 for α=20°. (Due to the limitation of the torque of the stepping motor, the optimum frequency at the maximum amplitude R=0.7 could not be reached). The optimum reduced frequency implies a special convective time scale which will be studied in detail later on. In figure 4, the phase-averaged lift coefficient $C_L(t)$ is shown as a function of time over a cycle for several values of the reduced frequency at R=0.59. Also shown is the steady-state lift coefficient. Note that during the acceleration, the lift coefficient can be roughly as twice as the steady one. This is due to the flow attachment. It is also known that pitching airfoils can produce higher lift coefficients and maintain flow attachment beyond the static stall angle[2]. During the deceleration, the phase-averaged lift coefficient increases and reaches its maximum values for the optimum reduced frequency $k=k_{opt}$. The maximum lift coefficients are around the middle of the cycle (t/T=0.5) which corresponds to the time when a large vortex is located just above the wing[9]. Flow visualization of three cases ($k<k_{opt}$, $k=k_{opt}$ and $k>k_{opt}$) for R=0.29 is shown in figure 5. For the optimum case $k=k_{opt}$, the shear layer is already separated from the leading edge at the beginning of the cycle (t/T=0). During the decelaration, a coherent vortex forms above the wing and becomes very strong in the middle of the cycle when the free stream velocity is minimum (t/T=0.5). For the larger reduced frequency ($k>k_{opt}$), the vortices are smaller in size and it is possible to observe two vortices above the wing. Note that a vortex is located on the wing during the acceleration which does not permit a complete attached flow as in $k=k_{opt}$. Because of this, the phase-averaged lift coefficient is lower during the acceleration (see figure 4). For $k<k_{opt}$, unsteady effects are not strong and the vortex is washed away quickly.

Effect of the reduced frequency on the lift force will be discussed with the aid of the schematics in figure 6. Since the vortical structures contribute to the aerodynamic forces, two parameters will be important. First is the relative time spent by a vortex around the airfoil. The vortices spend more time around the airfoil with increasing reduced frequency. The second parameter is the degree to which the vortices produce suction on the upper wing surface. This is related to curvature of streamlines around the airfoil. With increasing reduced frequency, the vortices become smaller and produce smaller curvature in outer the flow. Obviously, these two opposing effects make a compromise at the

optimum reduced frequency. As evidenced by the flow visualization (figure 5), the scale of the vortices is on the order of chord length when $k=k_{opt}$. This could be predicted by assuming a vortex convection speed ($U_C=K\ U_\infty$) and using the definition $k=\omega c/2U_\infty$. This provides $\lambda_{opt}/c=1.5$, based on the measurements[5] of K=0.40, and is in good agreement with the visual observations. For $k< k_{opt}$, the relative time spent by a vortex around the airfoil is small compared to the period of the velocity variations. On the other hand, for $k>k_{opt}$, the vortices induce only a small curvature in the outer flow.

2. *Effect of angle of attack*

In figure 7, the mean lift ratio defined as in (3) is shown as a function of the reduced frequency for different values of angle of attack in the poststall region. The static stall angle in this Reynolds number range is 12°. It is seen that there is an optimum reduced frequency for angles of attack larger than the static stall angle, although it is not a sharp peak for $\alpha=16°$. For $\alpha=12°$, there is no optimum reduced frequency. It should be also noted that the ratio $\overline{L(t)}/\overline{L_{qs}}$ is around unity for angles of attack smaller than the static stall angle[8]. This ratio was predicted to be unity for small angles of attack by thin airfoil theory[10].

The optimum reduced frequency is plotted as a function of angle of attack in figure 8, which suggests that the optimum reduced frequency is approximately independent of the angle of attack. Also shown is the Karman vortex street frequency in the wake of the airfoil in steady free stream. This measured values gives a Strouhal number $St=fc\sin\alpha/U_\infty=0.21$, which is in good agreement with the reported values[11] of $St\simeq 0.19$ for sharp-edged and rounded plates at similar aspect ratios. It is also known that streamwise oscillations of asymmetric bluff bodies in uniform stream may occur at natural shedding frequency or its second harmonic (not at the subharmonic), depending on whether the separated shear layer from leading-edge reattaches or not[12]. It should be kept in mind that these observations are for small amplitude oscillations. Since the flow has little similarity to a wake flow behind an airfoil (see flow visualization in figure 5) for large amplitude oscillations ($R\geq 0.29$), the optimum reduced frequency could not be related to wake instability.

It is also noted that optimum forcing frequencies were reported for airfoils at high angle of attack. These methods are based on forcing the separated shear layer (by sound[13] or oscillating wire[14]) in order to affect shear layer vortices. Optimum reduced frequencies in the range of k=3-9 were reported, which corresponds to separated shear-layer instability frequency[13]. The optimum reduced frequency found in this study is $k\approx 1$.

3. *Phase-averaged flow field*

The flow field at optimum reduced frequency (α=20°) for R=0.59 was studied in detail. Phase-averaged velocity vectors are shown in figure 9 at different phases of the cycle. At the beginning of the deceleration (t/T=0), the flow is already separated from the leading-edge and forms a separation bubble on the upper surface of the airfoil. During the decelaration, this bubble becomes a coherent vortex of increasing strength. Since the free stream velocity (or convection of vorticity) decreases while the shedding of vorticity from the leading edge continues, this results in accumulation of vorticity above the wing. The vortex reaches its climax around the middle of the cycle (t/T=0.5). With the increasing free stream velocity, the vortex is washed away from the airfoil. Note that a counter rotating vortex leaves the trailing-edge during the acceleration. Around t/T=0.875, the vortex is washed away completely and the flow around the airfoil is similar to an attached one. At this moment, the lift coefficient is roughly twice of the steady one (see figure 4).

The convection of the vortex along the airfoil at this optimum reduced frequency can be best illustrated with streamline patterns and vorticity field shown in Figure 10. Note that the vortex center is located just above the trailing-edge at t/T=0.5. It was noted earlier that the phase-averaged lift coefficient takes its maximum value at this moment. As will be shown in the next section, the strength (circulation) of the vortex also reaches its maximum around this moment. The vortex center deduced from the vorticity contours and streamline patterns is in good agreement, although this is not necessarily the case for unsteady flows. The vorticity contours also show opposite sign of vorticity on the upper surface during the deceleration.

4. *Effect of amplitude*

In this section, the effect of the amplitude at *optimum redeuced frequency* was investigated. The variation of phase-averaged lift coefficient for different values of amplitude R is shown in figure 11. Note that all lift coefficient curves collapse during the acceleration ($0.8 \leq t/T \leq 1.0$). This is due to the flow attachment (see phase-averaged velocity field in this time interval). It is expected that there is a lower value of amplitude below which the flow attachment is not possible. An example of small amplitude oscillations in poststall region was visualized by Brendel[15].

High lift coefficients which occur in the middle of the cycle increases very rapidly with increasing amplitude. Flow visualization for these cases is outlined in figure 12. Instantaneous flow field is shown at the beginning and middle of the cycle (t/T=0 and 0.5) for different values of amplitude R. Flow field does not seem to be affected much by amplitude. However, this conclusion based on flow visualization might be misleading. In order to get quantitative information, circulation measurements were carried out. The control surface was chosen based on flow visualization pictures in order to cover the large vortex. Figure 13 shows the control surface and variation of circulation ($\Gamma/U_\infty c$) which was calculated as a line integral. It should be noted that effects of location of

boundaries chosen was explored in initial experiments. Small changes (10%) in the location of three boundaries (upper, lower and inflow) do not effect the variation of circulation noticeably. The changes in the outflow boundary affect the time that the circulation drops rapidly, which indicates that the vortex has left the control surface. However, the maximum values remain very much the same. The circulation also reaches its maximum around the middle of the cycle. Figure 14 shows the variation of maximum circulation and the value at t/T=0.5. Finally, Figure 15 shows the variation of maximum lift coefficients and the time-averaged lift force ($\overline{L}/\frac{1}{2}\rho S U_\infty{}^2$) with the amplitude. The average force seems very large compared to average quasi-steady lift ($\overline{L_{qs}}/\frac{1}{2}\rho S U_\infty{}^2$) shown with dashed lines. Note that the time-averaged lift force varies almost linearly while a good curve fit to the maximum lift coefficient is $(C_L)_{max}=1.088/(1-R)^2$.

5. *Effect of leading-edge curvature*

In order to explore the degree to which the curvature of leading-edge may affect the vortex-airfoil interaction, a flat plate with sharp edge (chord length c=12.7 cm, therefore the same Reynolds number) was tested. The mean lift ratio defined as in (3) is compared with that of the NACA 0012 airfoil in figure 16 for $\alpha=20^\circ$. The solid and open symbols denote different amplitudes of oscillation (R=0.42 and R=0.59). The differences between the performance of a flat plate and the NACA 0012 seem little at small reduced frequencies and becomes larger with increasing reduced frequency. Nevertheless, overall character seems to be the same.

6. *Effect of unsteady stream on drag force*

Although no unsteady force measurements were taken for drag component, its time-averaged value was estimated from wake velocity measurements. The velocity measurements were taken at a downstream location $x/c\simeq 1$ (in midspan plane) and the mean value of the drag force was calculated from

$$\overline{D}=\rho\, b \int_{-\infty}^{\infty} \overline{u(u-U)}\, dy$$

where $(\overline{\ \ })$ denotes time-averaging and b is span of the airfoil. The results in nondimensional form ($\overline{D}/\frac{1}{2}\rho S\, U_\infty{}^2$) are presented together with average lift force ($\overline{L}/\frac{1}{2}\rho S\, U_\infty{}^2$) measurements (with the load cell) in figure 17 for $\alpha=20^\circ$ and R=0.59. The average drag force also shows a maximum at the optimum reduced frequency. However, the average drag force increases less rapidly with increasing reduced frequency than the average lift force does (which means an increasing $\overline{L}/\overline{D}$ ratio). This is most probably due to the reversed flow (hence negative skin friction) over the wing during the time interval when the vortex is located above the wing.

CONCLUSIONS

It was shown that the aerodynamic performance (both time-averaged and phase-averaged) is a very strong function of the reduced frequency in the poststall region. This is in contrast to attached flows such as slender delta wings or small angles of attack for which vortex shedding is not observed. There is an optimum reduced frequency at which the time-averaged lift force becomes maximum. The optimum reduced frequency does not depend on amplitude of oscillation and is approximately independent of angle of attack. Very high lift coefficients exceeding 10 can be observed at this reduced frequency. This high performance is due to a large coherent vortex which sheds from the leading edge and stays on the wing until the time when the free stream velocity is minimum. The optimum reduced frequency does not seem to be related to the wake instability, although the natural vortex shedding frequency and the optimum frequency are on the same order of magnitude. Observed high aerodynamic loads does not critically depend on leading-edge curvature.

ACKNOWLEDGEMENT

This work is supported by AFOSR Contract No. F49620-88-C-0061.
90-C-0038

REFERENCES

1. Wu, T.Y.T "Hydromechanics of swimming propulsion. Part I. Swimming of a two-dimensional flexible plate at variable forward speeds in an inviscid fluid", *J. Fluid Mechanics*, vol. 46, 1971, pp. 337-355.

2. McCroskey, W.J. "Unsteady airfoils", *Annual Review of Fluid Mechanics*, vol. 14, 1982, pp. 285-311.

3. Maresca, C., Favier, D. and Rebont, J. "Experiments on an airfoil at high angle of incidence in longitudinal oscillations", *Journal of Fluid Mechanics*, vol. 92, 1979, pp. 671-690.

4. Reynolds, W. C. and Carr, L. W., "Review of Unsteady, Driven, Separated Flows", AIAA Paper No. 85-0527, 1985.

5. Shih, C. "Unsteady aerodynamics of a stationary airfoil in a periodically-varying free stream", Ph.D. Thesis, 1988, University of Southern California.

6. Kruppa, E. W. "A wind tunnel investigation of the Kasper vortex concept", AIAA Paper 77-310.

AIAA 13th Ann. Meet., 1977, Washington, DC.

7. Saffman, P.G. and Sheffield, J.S. "Flow over a wing with an attached free vortex", *Studies in Applied Mathematics*, vol. 57, 1977, pp. 107-117.

8. Gursul, I., Lin, H. and Ho, C.M. "Vorticity dynamics of 2-D and 3-D wings in unsteady free stream", AIAA-91-0010, January 1991.

9. Gursul, I. and Ho, C.M. "High aerodynamic loads on an airfoil submerged in an unsteady stream", submitted to AIAA Journal, 1991.

10. Isaacs, R. "Airfoil theory for flows of variable velocity", *Journal of the Aeronautical Sciences*, 1945, pp. 113-117.

11. Abernathy, F.H. "Flow over an inclined plate", *Transactions of the ASME, Journal of Basic Engineering*, 1962, pp. 380-388.

12. Obasaju, E.D., Ermshaus, R. and Naudascher, E. "Vortex-induced streamwise oscillations of a square-section cylinder in a uniform stream", *Journal of Fluid Mechanics*, Vol. 213, 1990, pp. 171-189.

13. Hsiao, F.B., Liu, C.F. and Shyu, J.Y. "Control of wall-separated flow by internal acoustic excitation", *AIAA Journal*, Vol. 28, No. 8, 1990, pp. 1440-1446.

14. Bar-Sever, A. "Separation control on an airfoil by periodic forcing", *AIAA Journal*, Vol. 27, No. 6, 1989, pp. 820-821.

15. Gad-el-Hak, M. "Visualization techniques for unsteady flows: An overview", *Journal of Fluids Engineering*, Vol. 110, 1988, pp. 231-242.

LIST OF FIGURES

Figure 1: Unsteady water channel.

Figure 2 : Flow visualization of NACA 0012 at α=20° in steady free stream.

Figure 3: Variation of time-averaged lift force normalized by time-averaged quasi-steady lift force as a

function of reduced frequency for different amplitudes (α=20°).

Figure 4: Phase-averaged lift coefficient as a function of time over a cycle (R=0.59).

Figure 5: Flow visualization for different reduced frequencies (R=0.29).
Instantaneous streamline patterns at several phases during a cycle.

Figure 6: Effect of reduced frequency on overall flow pattern.

Figure 7: Variation of time-averaged lift force normalized by time-averaged quasi-steady lift force as a function of reduced frequency for several values of angles of attack (R=0.29).

Figure 8: Variation of optimum reduced frequency as a function of angle of attack.

Figure 9: Phase-averaged flow field at several phases of the cycle (α=20°, R=0.59).

Figure 10: Streamline patterns and vorticity field at several phases of the cycle. For contours of constant vorticity, outermost contour has the same absolute value $\omega^*=\omega c/U_\infty=10$ (dashed lines denotes opposite sign of vorticity); increment between contour lines is $\delta\omega^*=10$.

Figure 11: Effect of amplitude on variation of phase-averaged lift coefficient at optimum reduced frequency.

Figure 12: Effect of amplitude on flow pattern at optimum reduced frequency.

Figure 13: Control surface for circulation measurements (top); variation of circulation $\Gamma/U_\infty c$ over a cycle at optimum reduced frequency (bottom).

Figure 14 : Effect of amplitude on maximum circulation at optimum reduced frequency.

Figure 15: Effect of amplitude on time averaged lift force ($\overline{L}/\frac{1}{2}\rho S U_\infty^2$) and maximum lift coefficient.

Figure 16: Variation of time-averaged lift force normalized by time-averaged quasi-steady lift force as a function of reduced frequency for NACA 0012 and flat plate.

Figure 17: Variation of time-averaged drag force ($\overline{D}/\frac{1}{2}\rho S\ U_\infty^2$) and lift force ($\overline{L}$ /$\frac{1}{2}\rho S\ U_\infty^2$) as

a function of reduced frequency (α=20°, R=0.59).

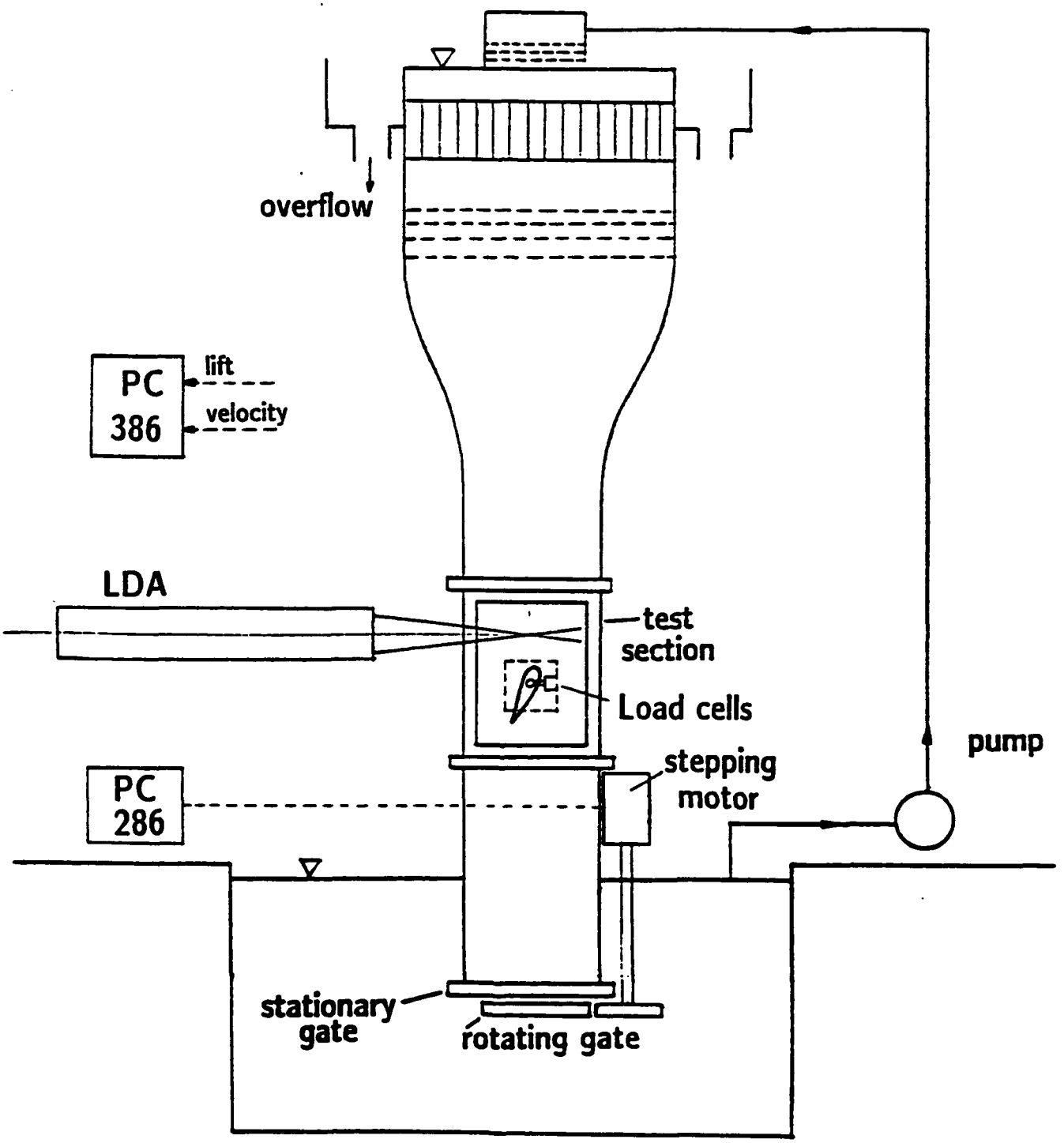

Figure 1: Unsteady water channel.

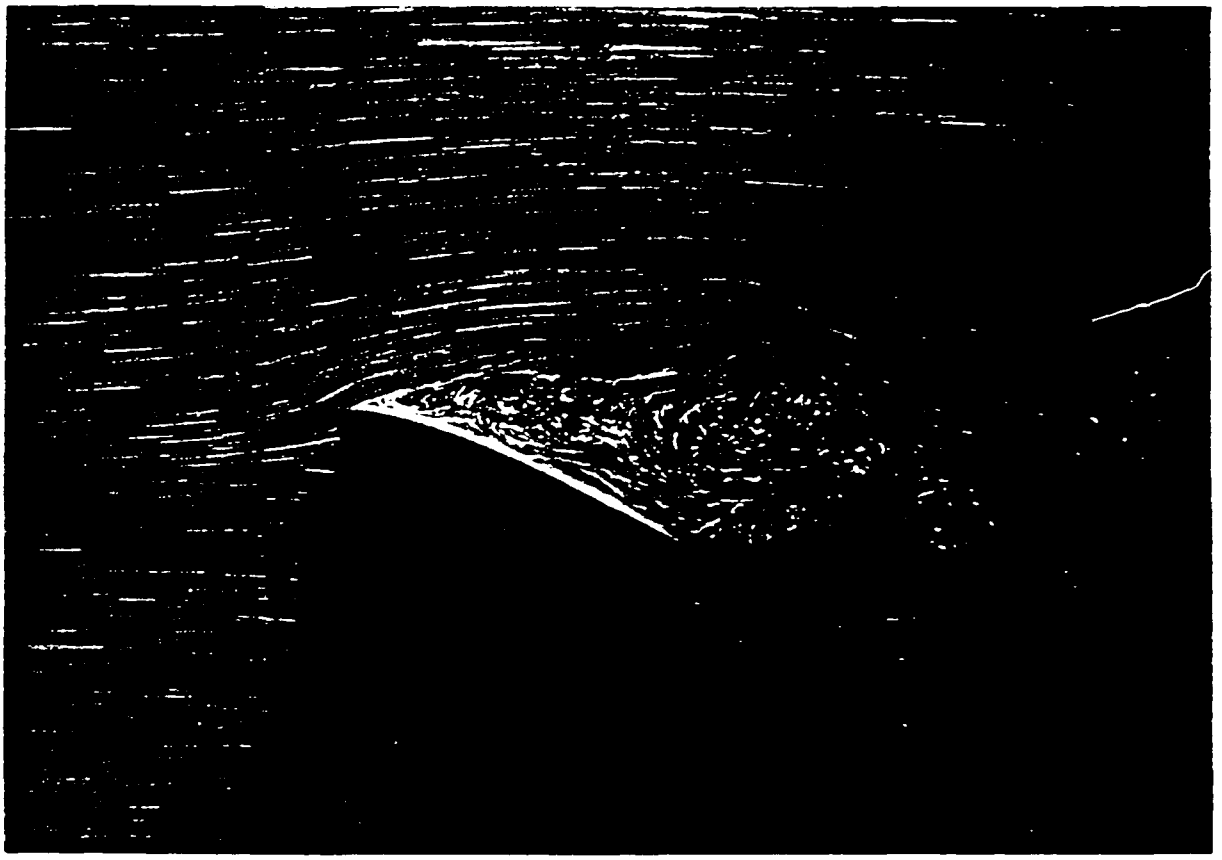

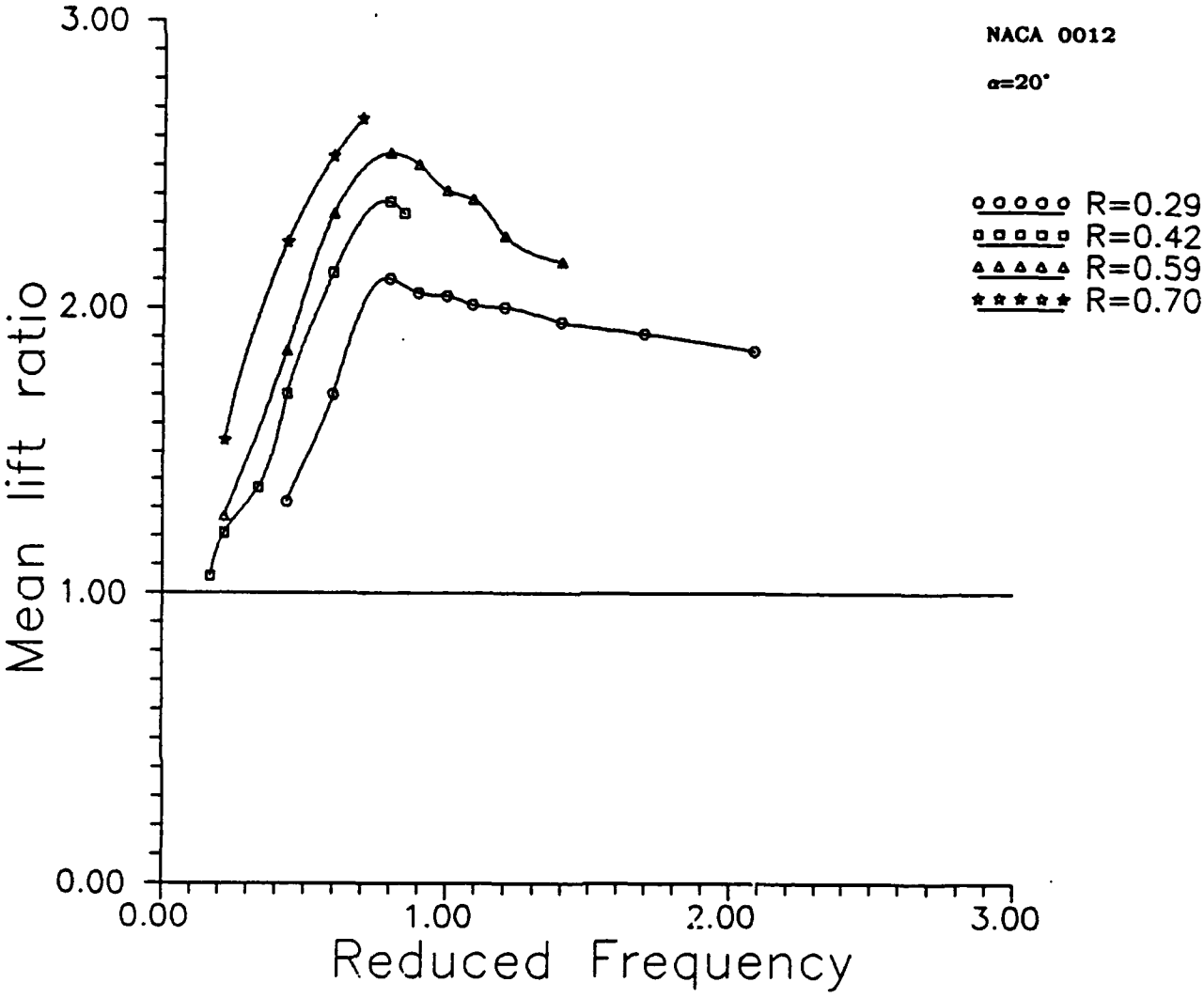

Figure 3: Variation of time-averaged lift force normalized by time-averaged quasi-steady lift force as a function of reduced frequency for different amplitudes (α=20°).

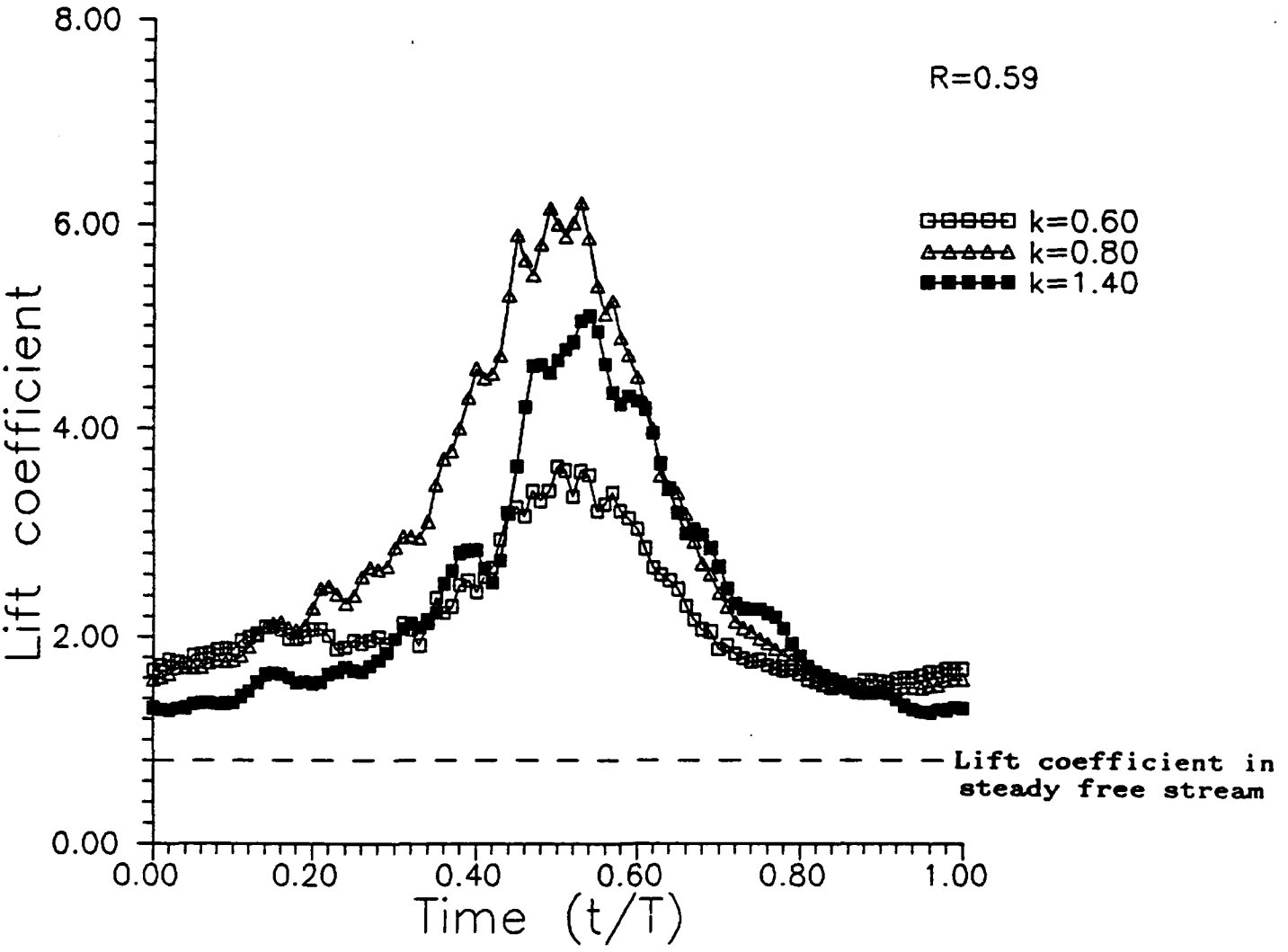

Figure 4: Phase-averaged lift coefficient as a function of time over a cycle (R=0.59).

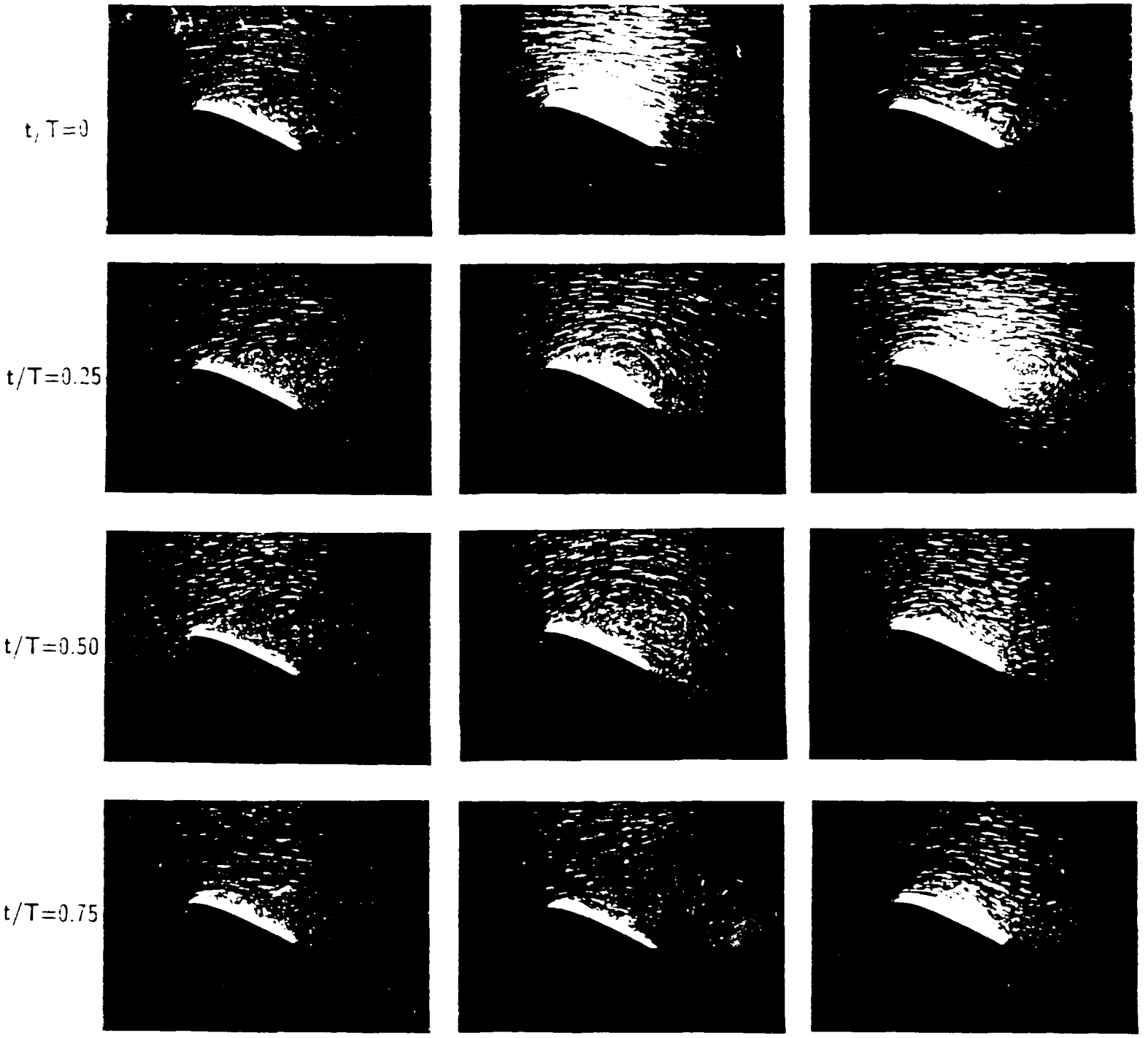
t, T=0
t/T=0.25
t/T=0.50
t/T=0.75
k=0.44
k=0.80
k=2.09
Cotimum reduced frequency

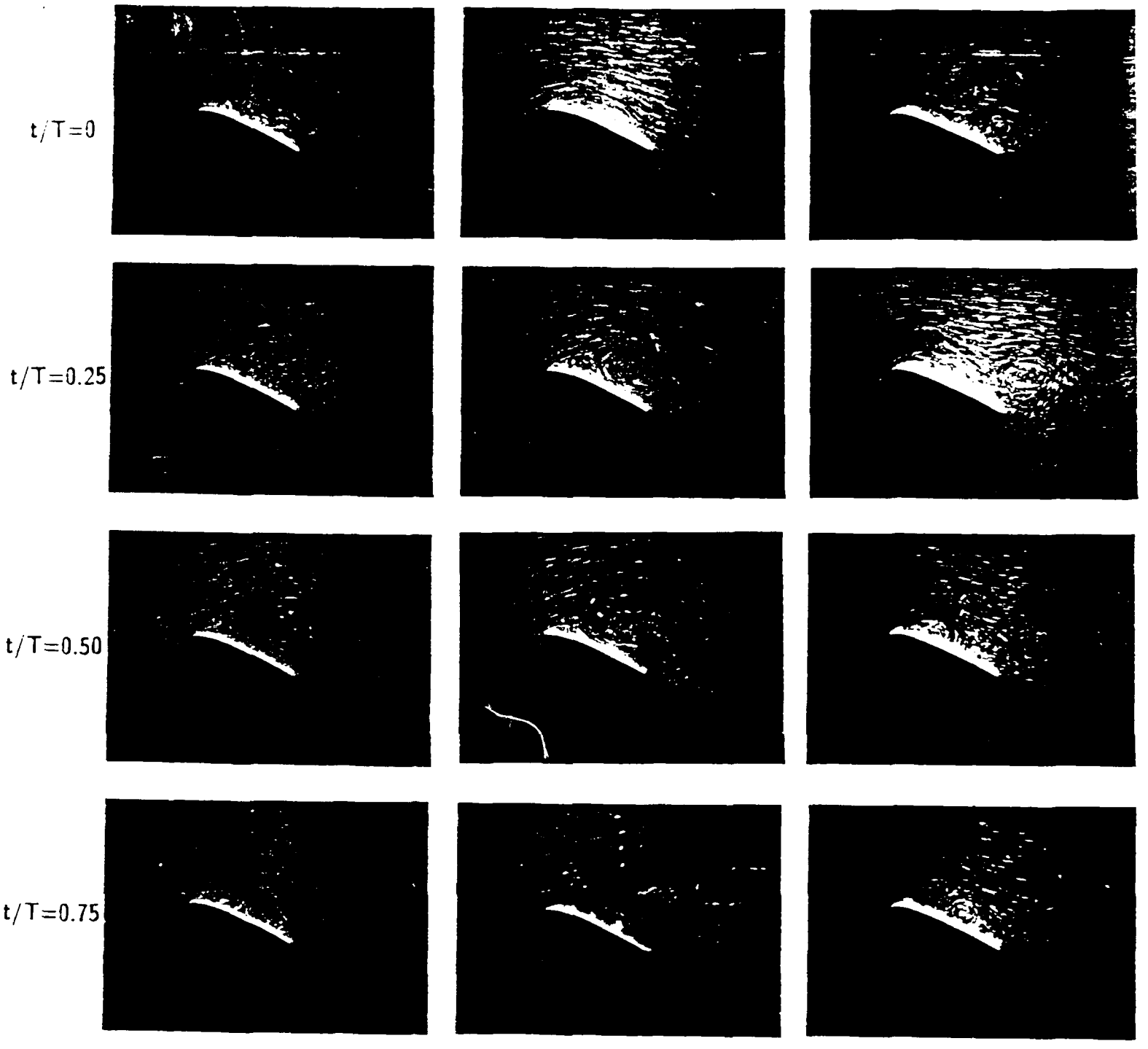

Optimum reduced frequency

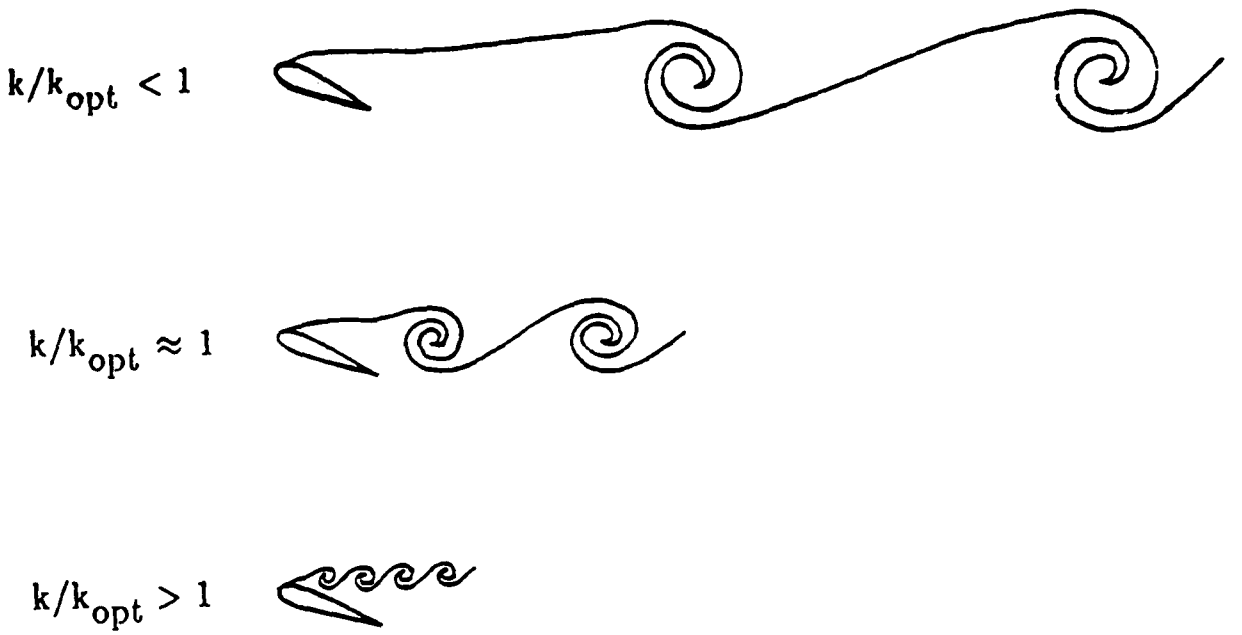

Figure 6: Effect of reduced frequency on overall flow pattern.

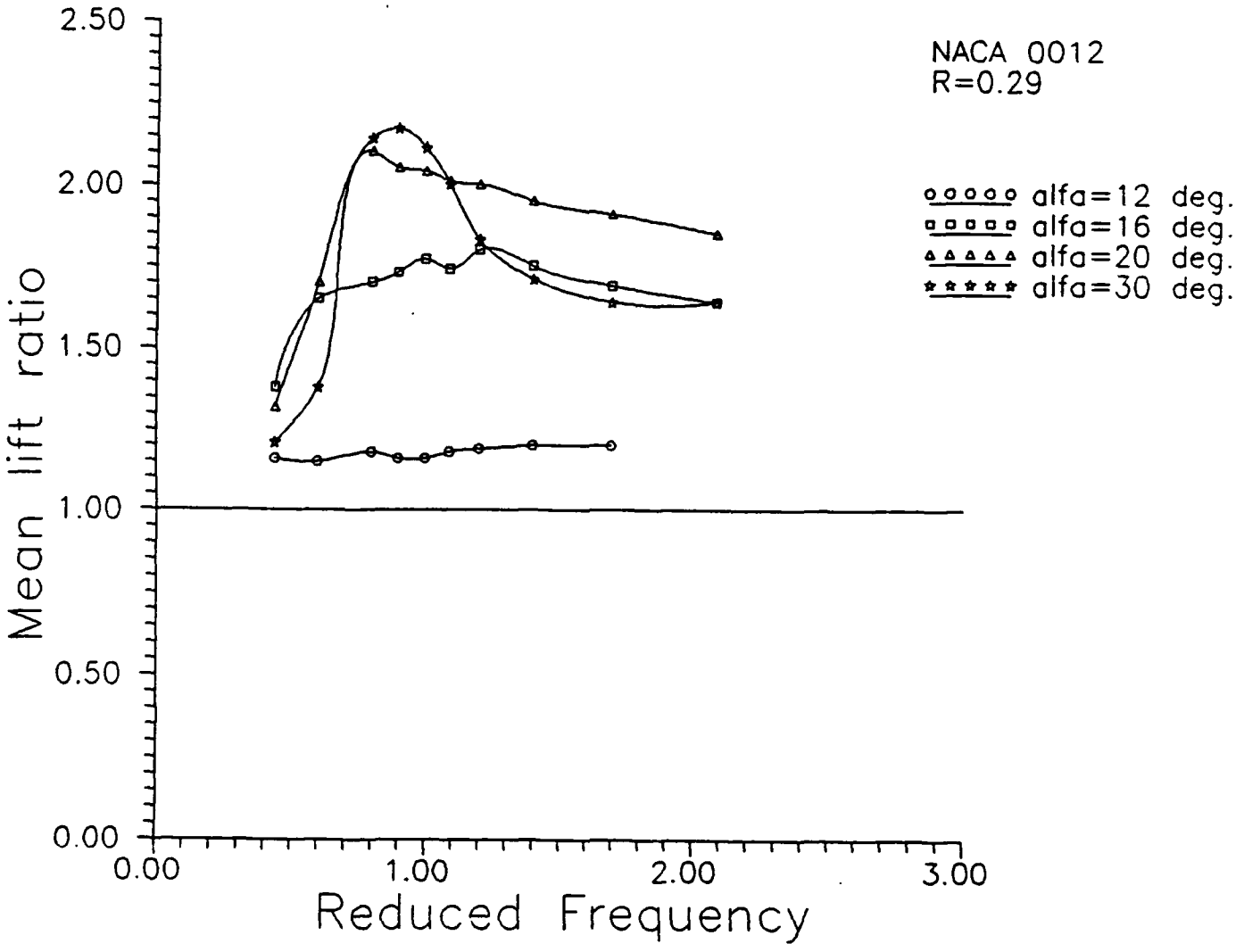

Figure 7: Variation of time-averaged lift force normalized by time-averaged quasi-steady lift force as a function of reduced frequency for several values of angles of attack (R=0.29).

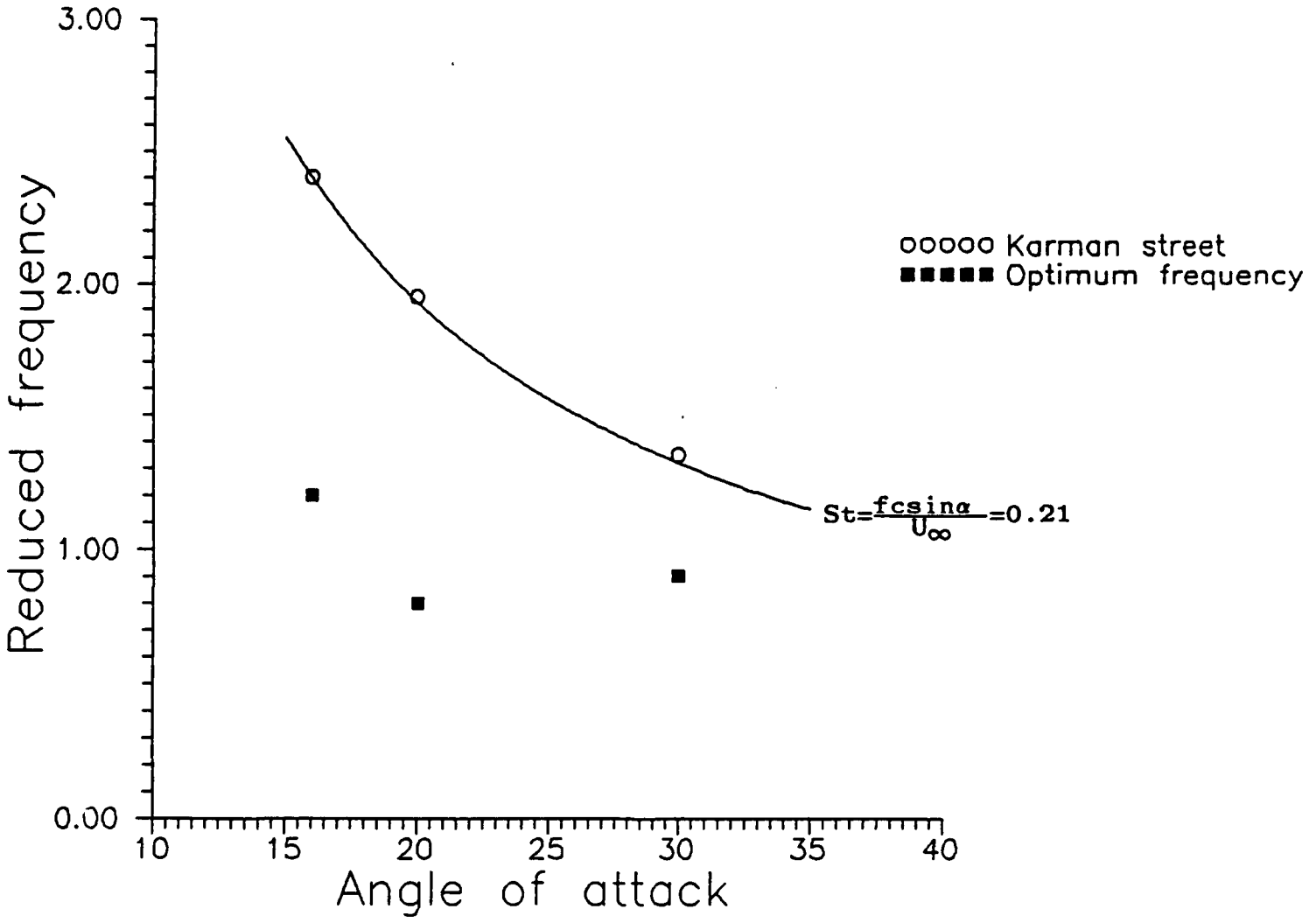

Figure 8: Variation of optimum reduced frequency as a function of angle of attack.

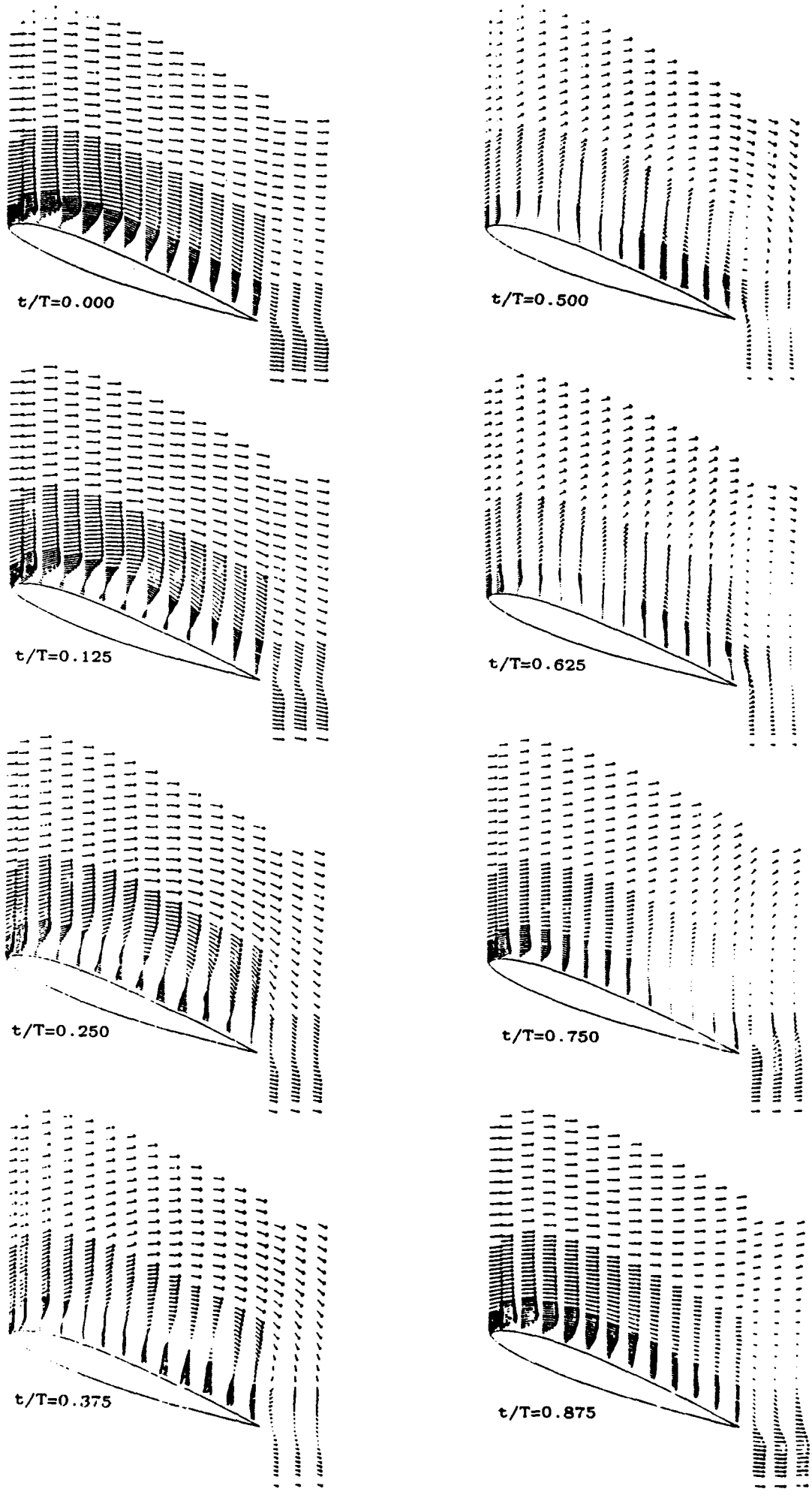

Figure 9: Phase-averaged flow field at several phases of the cycle (α=20°, R=0.59).

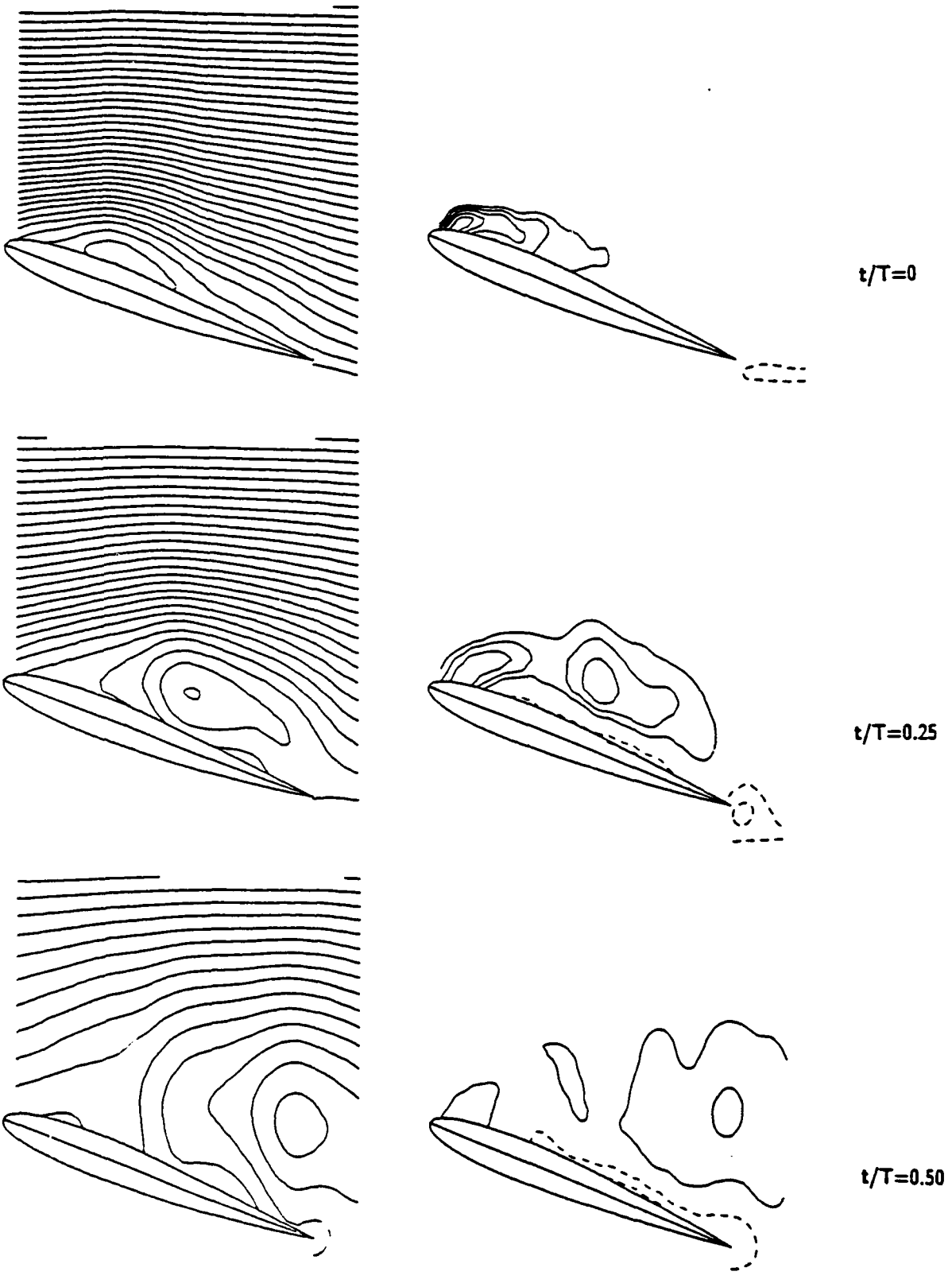

Figure 10: Streamline patterns and vorticity field at several phases of the cycle. For contours of constant vorticity, outermost contour has the same absolute value $\omega^*=\omega c/U_\infty=10$ (dashed lines denotes opposite sign of vorticity); increment between contour lines is $\delta\omega^*=10$.

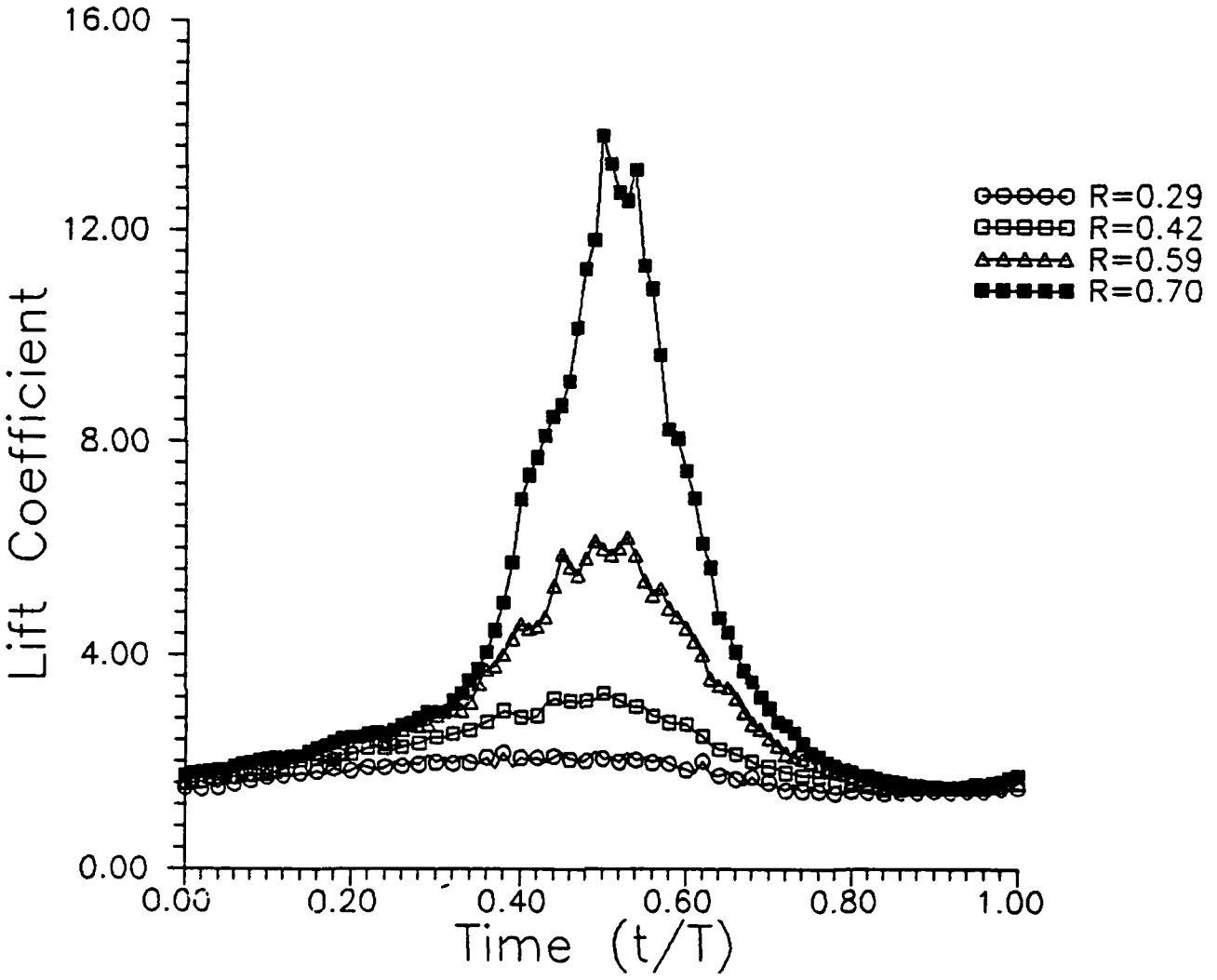

Figure 11: Effect of amplitude on variation of phase-averaged lift coefficient at optimum reduced frequency.

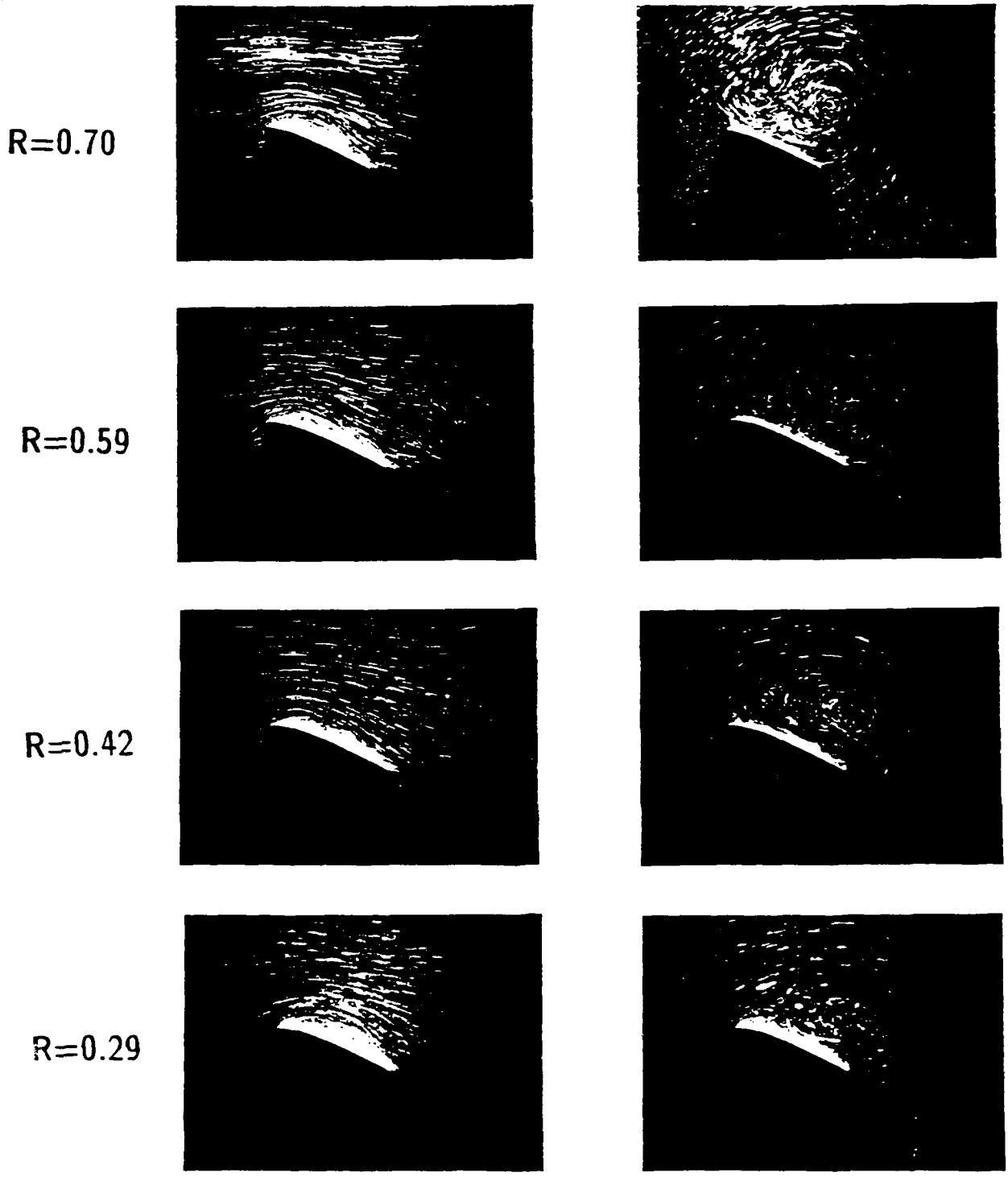

amplitude on flow

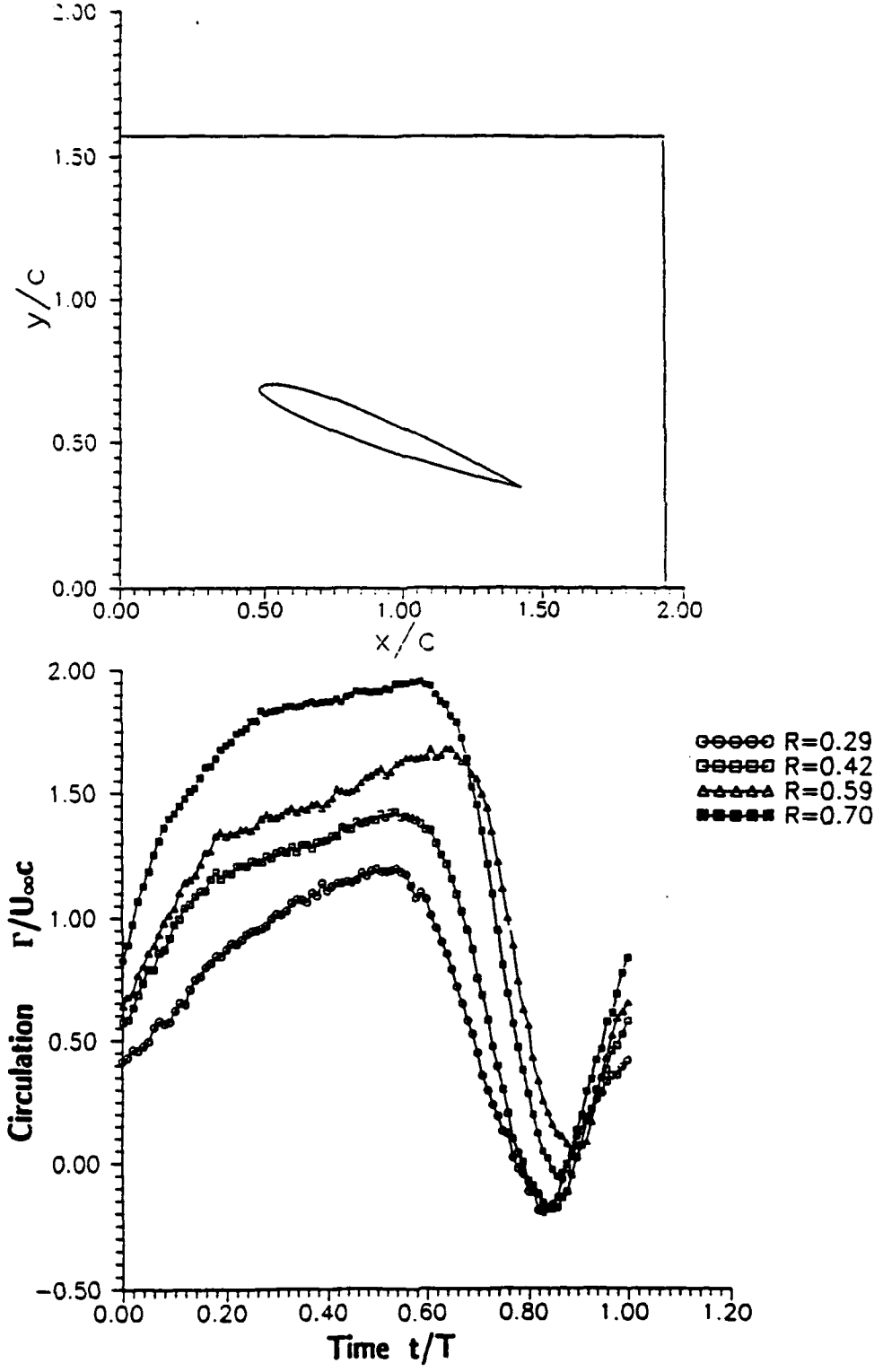

Figure 13: Control surface for circulation measurements (top); variation of circulation $\Gamma/U_\infty c$ over a cycle at optimum reduced frequency (bottom).

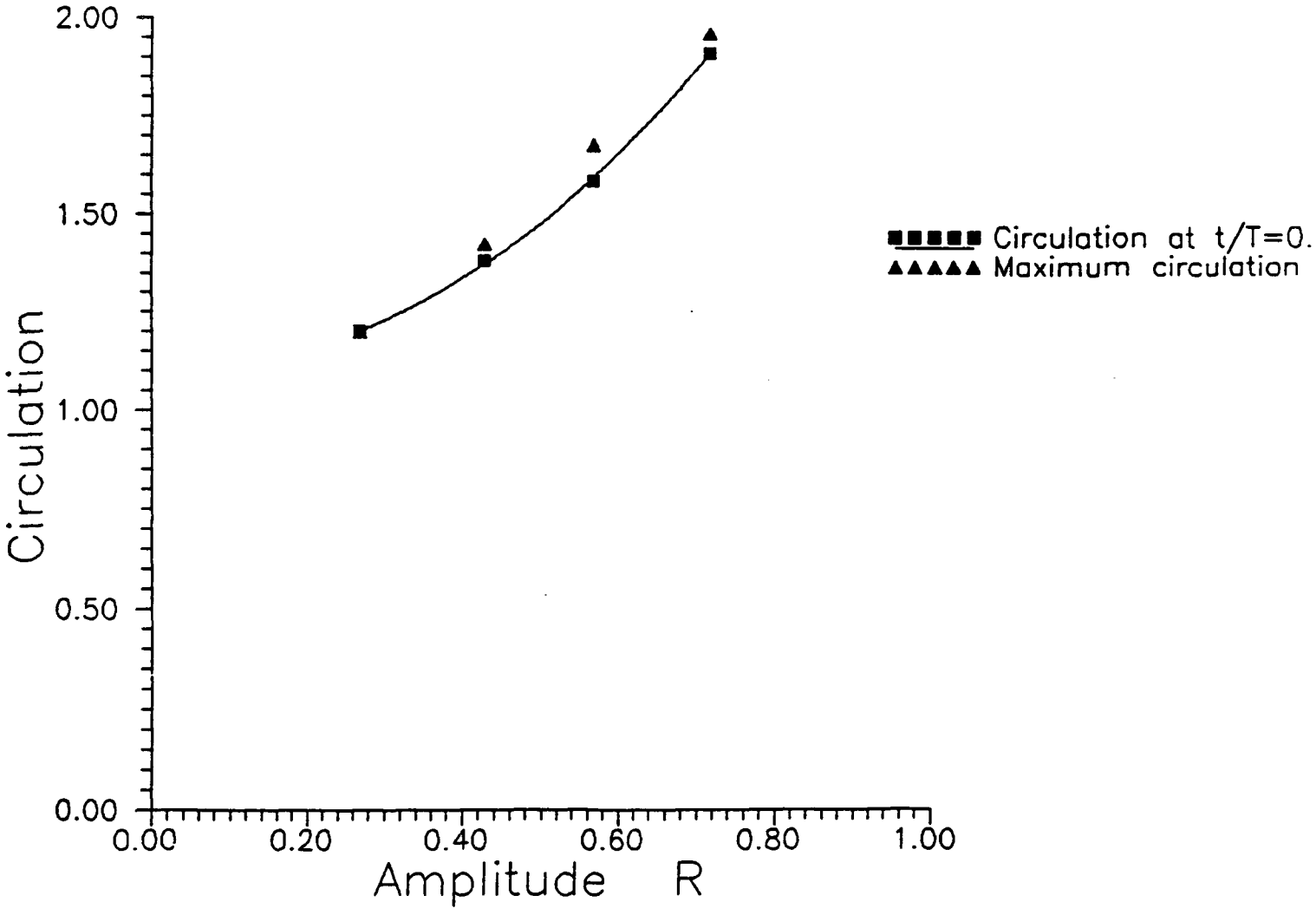

Figure 14 : Effect of amplitude on maximum circulation at optimum reduced frequency.

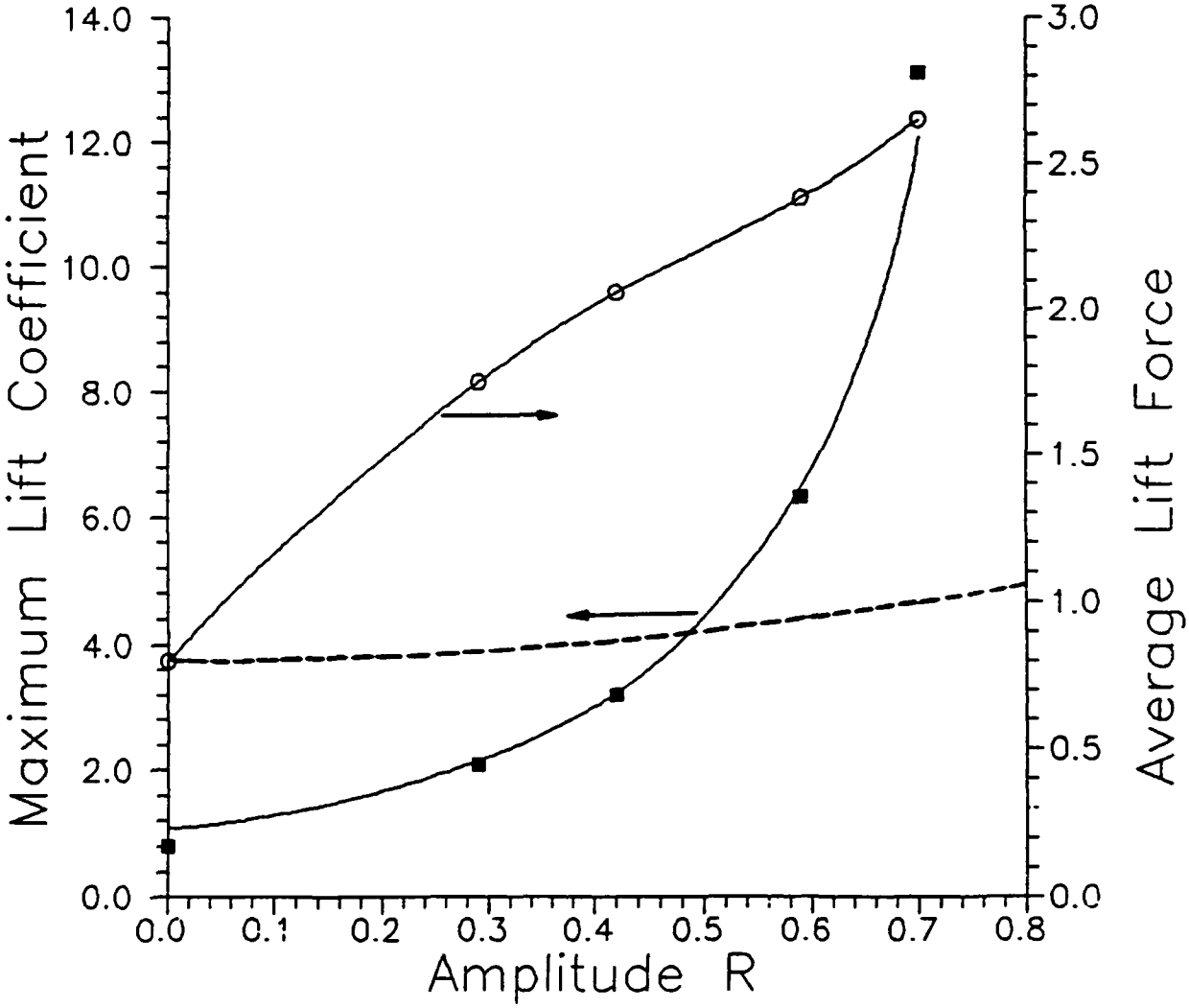

Figure 15: Effect of amplitude on time averaged lift force ($\overline{L}/\frac{1}{2}\rho SU_\infty{}^2$) and maximum lift coefficient.

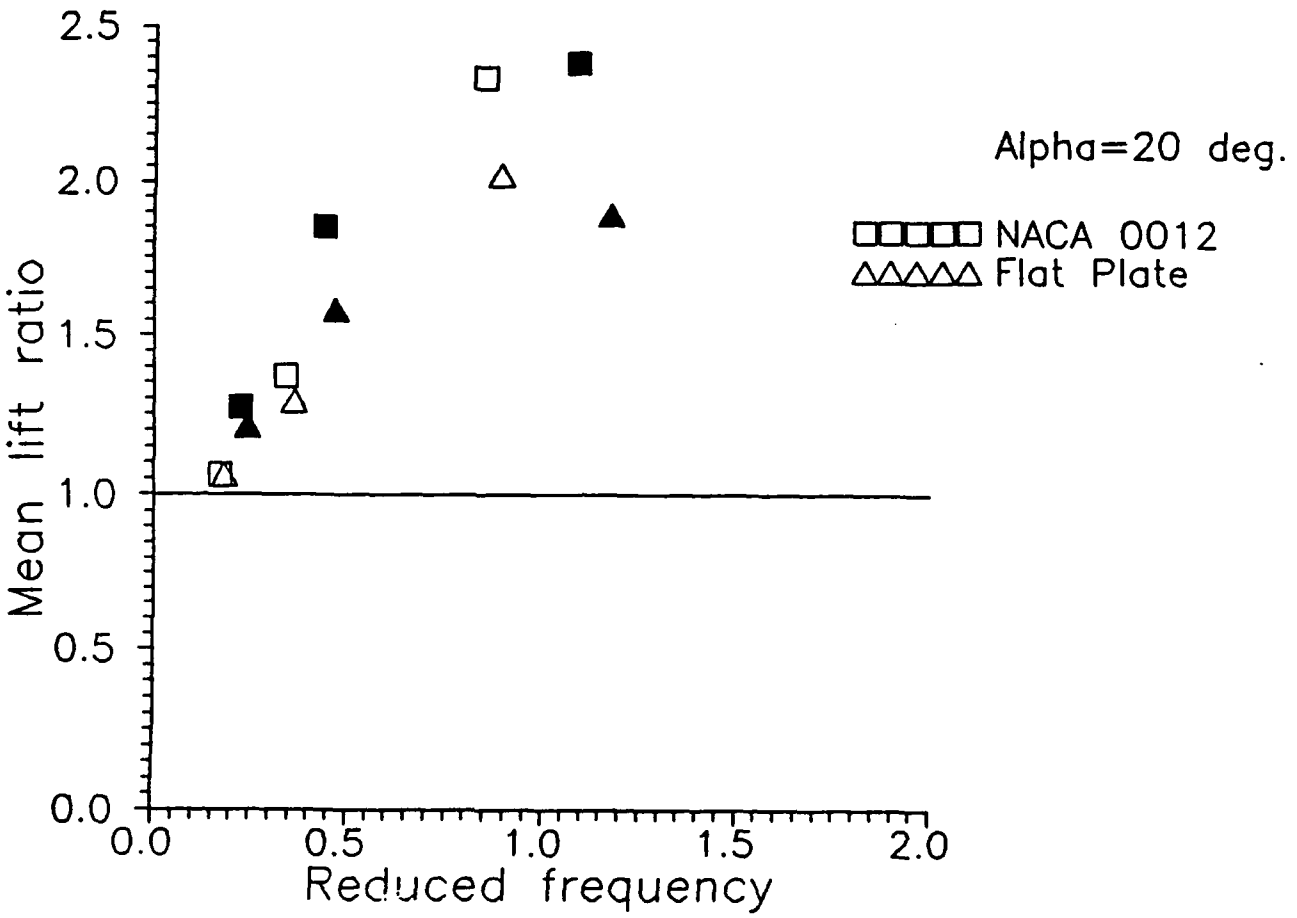

Figure 16: Variation of time-averaged lift force normalized by time-averaged quasi-steady lift force as a function of reduced frequency for NACA 0012 and flat plate.

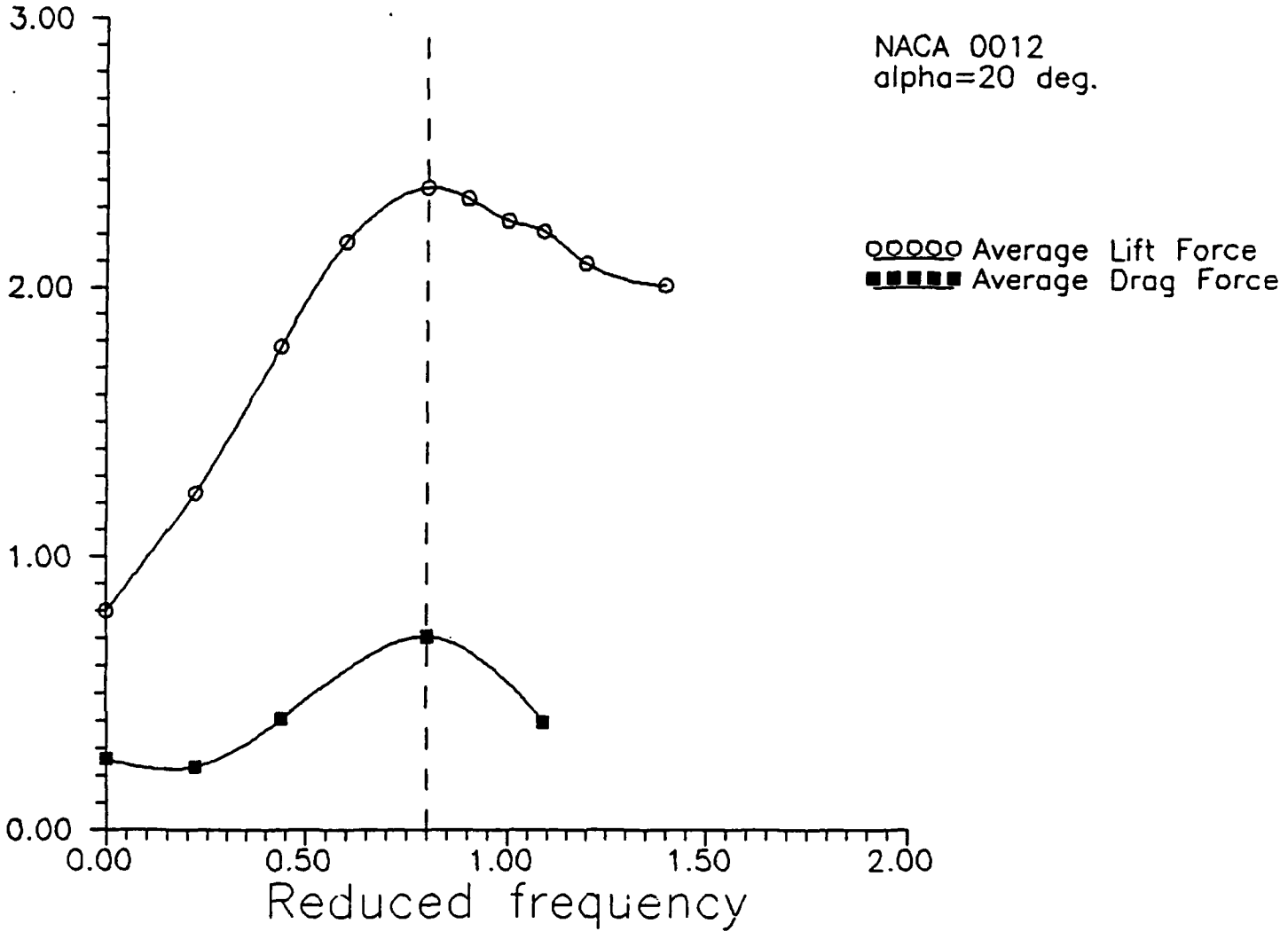

Figure 17: Variation of time-averaged drag force ($\overline{D}/\frac{1}{2}\rho S\, U_\infty{}^2$) and lift force ($\overline{L}/\frac{1}{2}\rho S\, U_\infty{}^2$) as a function of reduced frequency (α=20°, R=0.59).